University Of Alberta

Deposition of HVOF Overlay on Induction Hardened Steels

By

Lingyun Wei

A thesis submitted to the Faculty of Graduate Studies and Research in partial fulfillment of the requirements for the degree of Master of Science

In

Welding Engineering

Department of Chemical and Materials Engineering

Edmonton, Alberta

Spring 2004

Library and Archives Canada

Published Heritage Branch

395 Wellington Street
Ottawa ON K1A 0N4
Canada

Bibliothèque et Archives Canada

Direction du Patrimoine de l'édition

395, rue Wellington
Ottawa ON K1A 0N4
Canada

Your file Votre référence
ISBN: 0-612-96565-1
Our file Notre référence
ISBN: 0-612-96565-1

The author has granted a non-exclusive license allowing the Library and Archives Canada to reproduce, loan, distribute or sell copies of this thesis in microform, paper or electronic formats.

L'auteur a accordé une licence non exclusive permettant à la Bibliothèque et Archives Canada de reproduire, prêter, distribuer ou vendre des copies de cette thèse sous la forme de microfiche/film, de reproduction sur papier ou sur format électronique.

The author retains ownership of the copyright in this thesis. Neither the thesis nor substantial extracts from it may be printed or otherwise reproduced without the author's permission.

L'auteur conserve la propriété du droit d'auteur qui protège cette thèse. Ni la thèse ni des extraits substantiels de celle-ci ne doivent être imprimés ou aturement reproduits sans son autorisation.

In compliance with the Canadian Privacy Act some supporting forms may have been removed from this thesis.

While these forms may be included in the document page count, their removal does not represent any loss of content from the thesis.

Conformément à la loi canadienne sur la protection de la vie privée, quelques formulaires secondaires ont été enlevés de cette thèse.

Bien que ces formulaires aient inclus dans la pagination, il n'y aura aucun contenu manquant.

Canada

Abstract

Worn crankshaft journals with an induction-hardened surface layer are difficult to repair by High Velocity Oxy-Fuel (HVOF) powder metal overlays. The problems occur after cladding, and results in the overlays failing at the interface with the hardened surface, since the induction hardening has a deleterious effect on the surface preparation. Conventional tempering and intercritical induction heat treatments were assessed for modifying the surface hardness of the induction-hardened steel. Both processes are effective in reducing the surface hardness in short-time cycles by tempering the martensite. In addition, the intercritical induction heat treatment is then shown to be more effective for lowering surface hardness. The coating properties of the induction heat-treated crankshaft journals are evaluated by SEM. The adhesion strength of HVOF coatings is assessed by a modified ASTM Standard C 633-01 technique. The conclusion is that the crankshaft journals with the induction-hardened surface could be remanufactured by HVOF process after a short-time induction heat treatment process.

Acknowledgments

I would like to acknowledge the contributions of my supervisor, Dr. Barry M. Patchett for his guidance and support over the past few years, and also his supervision throughout the project.

Financial support was provided to this project by Headhunters Co. Ludwig & Associates Ltd. is gratefully acknowledged for assistance with the ASTM testing.

During the course of this research project, I would like to thank Bob Konzuk for his help and set up the induction furnace with the accessories. Tina Barker and Dongchen Lee performed the SEM analyses. I would like to thank Karen Koens in Ludwig & Associates who provided all-around help with tensile test needs and operations. I would also like to thank Ken Litchfield for spraying HVOF coating on all samples.

Table of Contents

1 Introduction 1

2 Literature Review 3

2.1 HVOF Spray Process 3

2.1.1 HVOF THEORY 4

2.1.2 HVOF Operation Technology 4

2.1.3 HVOF COATING STRUCTURE 7

2.1.4 HVOF Coating Materials 10

2.2 Steel Heat Treatment Processes 11

2.2.1 Carbon Steel 12

2.2.2 The Iron-Iron Carbide (Fe-Fe_3C) Phase Diagram 14

2.2.3 Furnace Heat Treatment Processes 29

2.2.4 Induction Heat Treating of Steel 30

2.3 ASTM Designation C633-01 36

2.3.1 Apparatus 36

2.3.2 Materials 37

2.3.3 Test specimen 38

2.3.4 Interpretation of Results 38

3 Objective 40

4 Experimental Procedure 42

4.1 Materials and Samples 42

4.2 Furnace Heat Treatment 43

4.2.1 Conventional Tempering Heat Treatment 43

4.2.2 Intercritical Heat Treatment 44

4.3 Induction Heating Treatment 44

4.3.1 Radio-Frequency Induction Furnace 45

4.3.2 Induction Heat Treatment 45

4.4 HVOF 46

4.5 Temperature Measurement for Induction Heating Treatment **47**
4.5.1 Thermocouples 48
4.5.2 Infrared Pyrometer 52
4.5.3 Tempil stick 54
4.6 Tensile Test **56**
4.6.1 Tensile Test Preparation 57
4.6.2 Test procedure 59
5 Results and Discussions **61**
5.1 Material for Initial Crankshaft Journal **61**
5.1.1 Microstructure 61
5.1.2 Hardenability 63
5.2 Hardness Analysis after Conventional Furnace Heat Treatment **63**
5.3 Hardness Analysis after Intercritical Furnace Heat Treatment **69**
5.4 Hardness Analysis after Induction Heat Treatment **73**
5.4.1 Reference Depth for Induction Heat Treatment 74
5.4.2 Experimental Data for Induction Heat Treatment 75
5.4.3 Microstructure Analysis after Induction Heat Treatment 79
5.5 HVOF **83**
5.5.1 Tensile Test Results and Discussion 84
5.5.2 Crankshaft Journal by Grit Blasting before HVOF Coating. 88
5.5.3 HVOF Coatings Properties 91
6 Conclusions **96**
7 Recommendations for Future Research **99**
8 Reference **100**

List of Tables

Table 2-1 Mechanical Properties for SAE 1040 (Ref. 9) 13

Table 2-2 Forging and Heat Treatment Parameters for SAE 1040 (Ref. 9) 13

Table 2-3 Chemical Composition of SAE 1040 (Ref. 9) 14

Table 2-4 Chemical Composition of SAE 1040 (Ref. 9) 20

Table 2-5 Approximate critical temperature for selected carbon and low-alloy steels (Ref. 14) 21

Table 4-1 Chemical Composition of SAE 1040 (Ref. 9) 42

Table 5-1 Surface Hardness of Samples after Furnace Tempering at 700 °C 64

Table 5-2 Surface Hardness of Samples after Furnace Tempering at 720 °C 64

Table 5-3 Surface Hardness of Samples after Furnace Tempering at 700 °C with preheating at 500 °C (Initial surface hardness is 525 Hv) 64

Table 5-4 Surface Hardness of Samples after Furnace Tempering at 720 °C with preheating at 500 °C (Initial surface hardness is 518 Hv) 64

Table 5-5 Surface Hardness of Samples after Furnace Tempering at 740 °C (Initial surface hardness is 518 Hv) 69

Table 5-6 Surface Hardness of Samples after Furnace Tempering at 750 °C (Initial surface hardness is 515 Hv) 69

Table 5-7 Microhardness data for the first group induction heat treatment (Initial surface hardness is 515 Hv) 75

Table 5-8 Microhardness data for second and third group experiments (Initial surface hardness is 518 Hv) 76

Table 5-9 Microhardness data for second and third group experiments 78

List of Figures

Figure 2-1 General types of thermal spray processes (Ref. 3) 5

Figure 2-2 Basic HVOF Process Operation (Ref. 3) 7

Figure 2-3 Schematic representation of a typical thermal spray powder consolidation process (Ref. 5) 8

Figure 2-4 Photomicrograph showing the microstructure of a thermally sprayed 80/20 NiCr alloy (Ref. 3) 9

Figure 2-5 The Fe-C equilibrium diagram up to 6.67% wt%. Solid lines indicate Fe-Fe_3C diagram; dashed lines indicate iron-graphite diagram. (Ref. 10) 14

Figure 2-6 Demonstration of how an isothermal transformation diagram (bottom) is generated from percent transformation-versus-logarithm of time measurements (top). (Ref. 13) 17

Figure 2-7 The effect of percentage substitutional elements in steel on the carbon content of the eutectoid point (Ref. 15) 19

Figure 2-8 The effect of percentage substitutional elements in steel on the temperature of the eutectoid transformation point (Ref. 15) 19

Figure 2-9 Photomicrograph of α Ferrite (90x). (Copyright 1971 by United States Steel Corporation.) (Ref. 14) 23

Figure 2-10 Replica transmission electron micrograph showing the structure of bainite. A grain of bainite passes from lower left to upper right-hand corners, which consists of elongated and needle-shaped particles of Fe_3C within a ferrite matrix. The phase surrounding the bainite is martensite. (Ref. 17) 24

Figure 2-11 Effect of carbon content on the structure of martensite in plain-carbon steels-lath type (Ref. 19) 25

Figure 2-12 Effect of carbon content on the structure of martensite in plain-carbon steels-mixed lath and plate types, arrow points to a plate (Ref. 19) 26

Figure 2-13 Effect of carbon content on the structure of martensite in plain-carbon steels-plate type (Ref. 19) 26

Figure 2-14 Photomicrograph showing the martensitic microstructure. The needle-shaped grains are the martensite phase, and the white regions are austenite that failed to transform during the rapid quench. (x 1220) (Photomicrograph courtesy of United States Steel Corporation.) (Ref. 19) 27

Figure 2-15 Electron micrograph of tempered martensite. Tempering was carried out at 594 ° C (1100° F). The small particles are the cementite phase; the matrix phase is α ferrite. 9300* (Copyright 1971 by United States Steel Corporation.) (Ref. 14) 28

Figure 2-16 Photomicrograph of a eutectoid steel showing the pearlite microstructure consisting of alternating layer of α ferrite (the light phase) and Fe_3C (thin layers most of which appear dark), (500*). (Ref. 20) 28

Figure 2-17 Induced eddy current in the specimen is opposite to that in the coil (Ref. 21) 32

Figure 2-18 Schematics showing current density characteristics. (Ref. 21)) 33

Figure 2-19 Reference depth for various materials (Ref. 23) 34

Figure 2-20 Self-Aligning Device and Test Assembly View (Ref. 26) 37

Figure 2-21 Substrate and Loading Fixture (Ref. 26) 39

Figure 4-1 Crankshaft Journal Sample and Pie-shaped samples cut from Crankshaft Journal 42

Figure 4-2 Experiment setting up for K-type Thermocouple without Isolation cover 49

Figure 4-3 Temperature Measurement by K-type Thermocouple without Non-conductive cover 50

Figure 4-4 K-type Thermocouple with Non-conductive Tube 51

Figure 4-5 Experiment set-up for K-type Thermocouple with Non-conductive Tube 51

Figure 4-6 Temperature Measurement by K-type Thermocouple without Non-conductive Cover 52

Figure 4-7 OMEGA OS523-3 Infrared Pyrometer (Ref. 30) 53

Figure 4-8 Field of View for OMEGA OS523-3 (Ref. 30) 54

Figure 4-9 Self-Aligning Device for Tensile Test by Headhunters Co. 58
Figure 4-10 The Contour of the Loading Fixture 58
Figure 4-11 The Vertical View for the Loading fixture 59
Figure 4-12 Coated substrate with cylindrical loading fixture are mounted in the Alignment Device 59
Figure 4-13 The figure for attaching the loading fixture to the coated crankshaft journal 60
Figure 5-1 Microstructure for Initial Crankshaft surface by SEM (x1500) 62
Figure 5-2 Microstructure for Initial Crankshaft surface by Microscope (x 630) 62
Figure 5-3 Surface Hardness after Conventional Furnace Heat Treatment 65
Figure 5-4 Microstructure for tempering at 720 °C (x 630) 68
Figure 5-5 Microstructure for tempering at 700 °C (x 630) 68
Figure 5-6 Surface Hardness after Intercritical Furnace Heat Treatment 70
Figure 5-7 Microstructure for Intercritical Heat Treatment @ 740 °C-5 min. (x 630) 72
Figure 5-8 Microstructure for Intercritical Heat Treatment @ 750 °C-5 min. (x 630) 73
Figure 5-9 Electrical Resistivity of Steels (Ref. 36) 75
Figure 5-10 Surface Hardness after Induction Heat Treatment 76
Figure 5-11 Microstructure for 60-seconds Induction Heating Process by SEM (x1500) 81
Figure 5-12 Microstructure for Induction Tempering Heat Treatment (704 °C) 82
Figure 5-13 Microstructure for Induction Intercritical Heat Treatment (732 °C) 82
Figure 5-14 Image of Fracture Surface for HVOF Sample after Tensile Test 85
Figure 5-15 SEM for Fracture Surface after Tensile Test (x400) 86
Figure 5-16 SEM for Fracture Surface after Tensile Test (x150) 86
Figure 5-17 Initial Crankshaft after grit blasting 89

Figure 5-18 Induction-heated Crankshaft after grit blasting..... 89
Figure 5-19 Surface morphology of the Initial Hardened Crankshaft after Grit Blasting (x200)..... 90
Figure 5-20 Surface morphology of the Induction Heated Crankshaft after Grit Blasting (x200)..... 91
Figure 5-21 Cross Sectional Scanning Electron Micrograph of the as-sprayed coatings (x 50)..... 92
Figure 5-22 Cross Sectional Microstructure of Interface layer between HVOF coating and Crankshaft Surface (x 150)..... 93
Figure 5-23 Cross Sectional SEM image for HVOF Coating (x300)..... 94
Figure 5-24 SEM image of Surface Morphology for HVOF Coating (x500)..... 95

List of Symbols

Symbol	Meaning
ASTM	American Society for Testing and Materials
Hv	Hardness Vickers
HVOF	High Velocity Oxy-Fuel
Metco	Sulzer Metco Inc. (The Coatings Company)
SAE	Society of Automotive Engineers
SEM	Scanning Electron Microscope
UNS	Unified Numbering System

1 Introduction

Wear resistant coatings are of great importance to industry. In this particular instance, the use of overlays on crankshaft journals to repair worn parts of stationary engines is an effective method of renewing engines. Some crankshafts (usually of SAE 1040 carbon steel) are used as-machined and can be repaired easily using high velocity oxy-fuel (HVOF) power metal overlays. However, other engine manufacturers use the same steel, but add induction hardening on the journal surface. Induction hardening has a deleterious effect on the HVOF repair, which results in the overlay failing at the interface with the hardened steel of the crankshaft journal. The hardened surfaces do not permit grit blasting with Al_2O_3 particles to develop a suitably rough surface for bonding the overlay.

The objectives of this project are to identify short and simple thermal processes that will mitigate the effects of induction hardening on the application of HVOF overlays for the repair of worn crankshafts. The furnace heat treatments were tried on the crankshaft journals which proved whether short-time conventional and intercritical heat treatments are effective to lower the surface hardness. Then induction heat treatments were conducted to determine the required short-time heat treating process to lower the surface hardness effectively. Finally, the properties of HVOF coating for the induction-heated crankshaft were evaluated by SEM and modified ASTM C 633-01 tensile tests standard.

A literature review of the factors affecting HVOF overlays for the repair of worn crankshafts is covered in Chapter 2. It includes HVOF process, furnace heat treatments and induction heating processes. The objective of this project is stated in Chapter 3. The

experimental procedures used in the project are outlined in Chapter 4. Chapter 5 presents the results of the study in terms of the surface hardness after the heat treatment processes, the adhesion strength of HVOF coatings and the SEM microstructures of the coatings-coated interface. Conclusions found regarding deposition of HVOF Overlay on Induction Hardened Steels are given in Chapter 6. Chapter 7 is the recommendations for future work.

2 Literature Review

In today's competitive world, reducing operation costs while maintaining operation time can mean the difference between success and failure. Prices on new replacement parts are quite expensive, and there's also downtime, delivery, and quality to consider. It often is more economical to resurface worn parts than to replace them. Therefore, remanufacturing parts is an effective industrial procedure.

In industry, it is frequently necessary to build up surfaces that have been worn down, incorrectly cast, or incorrectly machined. For this particular case, the use of overlays on crankshaft journals to repair worn parts of stationary engines is an effective method of renewing engines. HVOF is the technique of choice in many of these instances. This chapter discuss details of HVOF spray process and other related knowledge.

2.1 HVOF Spray Process

The rapid advancement of High Velocity Oxy-Fuel (HVOF) spray coating technology has led to many diverse applications since its introduction over 10 years ago. (Ref. 1) The HVOF process is used widely in the aeronautics industry, oil and petroleum equipment, turbines, etc. This process can be used - depending on the powder properties (ceramics, metals, carbides, self-fluxing powders) - with various fuel gases such as Hydrogen, Acetylene, LPG's, Kerosene or SPRAL™ (SPRAL™ is a range of coating gases for conventional processes wire coatings or for High Velocity Oxy-Fuel and Plasma coatings). The application of HVOF coatings has several advantages, which including a

low equipment installation cost, a uniform coating thickness, no problems with waste disposal, a rapid deposition rate and significant process mobility. (Ref. 1)

2.1.1 HVOF THEORY

HVOF spraying theory is quite basic. Hot combustion gases are channeled and combined with a fine metal powder and accelerated down a nozzle. This process requires compressed air, a fuel gas and oxygen to be mixed in controlled quantities, the mixture being ignited in a spray gun. Water and the coating powder are then injected into the lighted plume of the spray gun. As the particles are melted and accelerated towards the surface to be coated, they heat up, soften and deposit themselves onto the surface. The powder particles impact the work piece, where they are deformed and quenched. The combustion temperature is approximately 5000°F (2760°C) with exhaust velocities up to 1400 meter/second (4500 feet/second). This method of thermal spraying provides coating properties that exhibit high density and uniformity. (Ref. 2)

2.1.2 HVOF Operation Technology

All thermal spray methods use chemical or electrical energy to heat feed materials injected into hot-gas jets to create a stream of molten droplets that are accelerated and directed toward the substrates being coated. Figure 2-1 shows how various thermal spray processes can be broken down according to the energy source used (combustion versus electrical), feed material form (powdered or solid), and surrounding environment (air, low pressure [vacuum], inert gas, etc.). (Ref. 3) HVOF is one kind of the combustion spray process with using powdered feed materials.

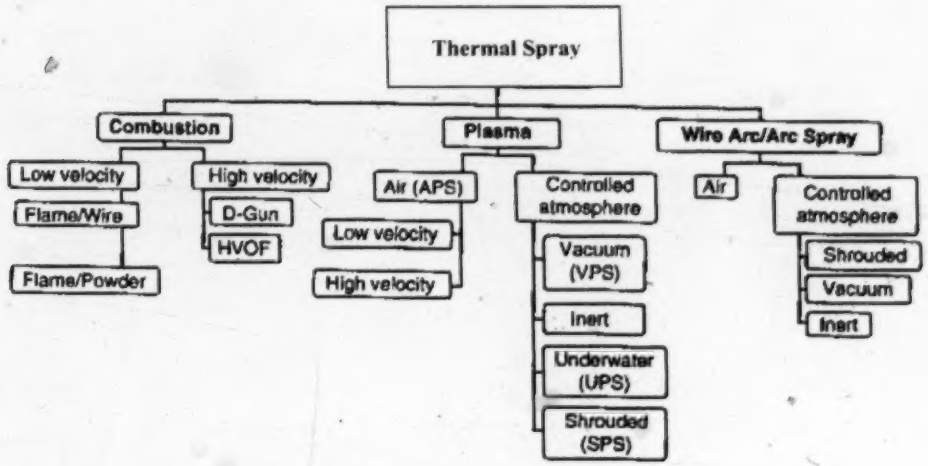

Figure 2-1 General types of thermal spray processes (Ref. 3)

2.1.2.1 Preparation for substrate surface before HVOF

Metal powder coating by HVOF spraying methods are bonded to the substrates by mechanical interlocking force. To improve the adhesive strength of the coating, the control of the surface geometry of the substrates is one of the important approaches. Generally, the substrate surface is cleaned and roughened by grit blasting before spraying.

Pre-cleaning includes degreasing and cleaning paint and rust from the surface. For a workpiece with grease, an effective cleaning method is heating the cast, and then cleaning it by detergent or solvent. For oxide and rust on the substrate surface, it may be cleaned by peening, grinding and cutting. (Ref. 4)

Grit blasting is the most common method for preparing the substrate surface prior to coating. The purposes for surface preparation are:

- To roughen the substrate surface, which will improve the adhesion strength of the coating to the substrate. (The roughened substrate surface is modeled by a series of circular arcs which supply more attachment surfaces for HVOF process.)
- To clean the substrate surface, which ensures the quality of surface, and removes fatigue and corrosion layers, carburised layers and so on.
- To modify an unevenly worn surface, allowing a uniform coating thickness.

The grit blasting finishing process blasts abrasive particles onto the substrate surface in order to produce a roughened surface. The grit may consist of iron, aluminium oxide, silicon dioxide or any crushed or irregular abrasive. The selection of the grit depends on the hardness of substrate being coated. For hard cast iron grit, the maximum surface hardness substrate to be grit blasted is roughly HRC 50 (513 Hv). Using aluminium oxide, surface hardness up to HRC 40 (392 Hv) could be grit blasted. Using silicon dioxide, the maximum surface hardness is below approximately HRC 30 (302 Hv). (Ref.4) In this project, alumina particles were used to blast the surface of a journal to roughen the surface and provide "tooth" for the cladding alloy to bond to the surface. The surface maximum hardness is 300 Hv. This hardness is normal for non-induction hardened surfaces of SAE 1040 steel. Alumina grit blasting is not effective on induction-hardened surfaces which have surface hardness over 500 Hv.

2.1.2.2 Basic Principles of Operations Technology

The HVOF unit uses an oxygen-fuel mixture with the fuel consisting of propylene, propane, or hydrogen to produce the highest quality coating depending on coating requirements. Fuel gases are mixed in a proprietary siphon system in the front portion of

the HVOF gun. The thoroughly mixed gases are ejected from the nozzle and ignited externally. Ignited gases form a circular flame configuration that surrounds the powdered material as it flows through the gun. The circular flame shapes the powder stream to provide uniform heating, melting, and acceleration Figure 2-2 shows the basic HVOF process operation. (Ref. 3)

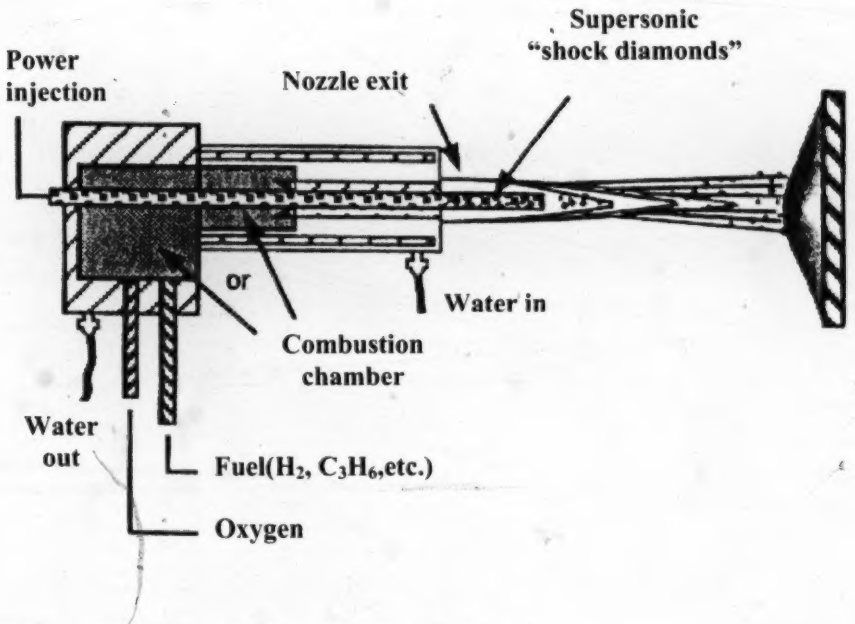

Figure 2-2 Basic HVOF Process Operation (Ref. 3)

2.1.3 HVOF COATING STRUCTURE

Thermal Spray is a "family" of particulate/droplet consolidation process that is capable of forming metals, ceramics, intermetallics, composites, and polymers into coatings. During the HVOF process, powders, wires, or rods are injected into the combustion zone. The fine dispersion of droplets is heated, melted or softened, accelerated to velocities in the

range 50 to >2000 m/s, and directed toward the surface of substrate being coated. On impact at the substrate, the particles or droplets rapidly solidify, cool, and contract, and incrementally build up to form a deposit. The thin "splats" undergo very high cooling rates, typically in excess of 10^6 K/s for metals. (Ref. 5) The high particle temperatures and velocities achieved result in significant droplet deformation on impact at a surface, producing thin lamellae layers, which conform and adhere to the substrate surface. Individual splats are generally thin (1 to 20 μm). (Ref. 5) Figure 2-3 shows a schematic of a generic thermal spray powder consolidation process, illustrating a typical deposit microstructure. Sprayed deposits usually contain some level, typically between 0 and 10% of porosity, some unmelted or partially melted particles, fully melted and deformed "splats", and some oxidation resulted from the hot coating particles reacted with the surrounding air. (Ref. 3)

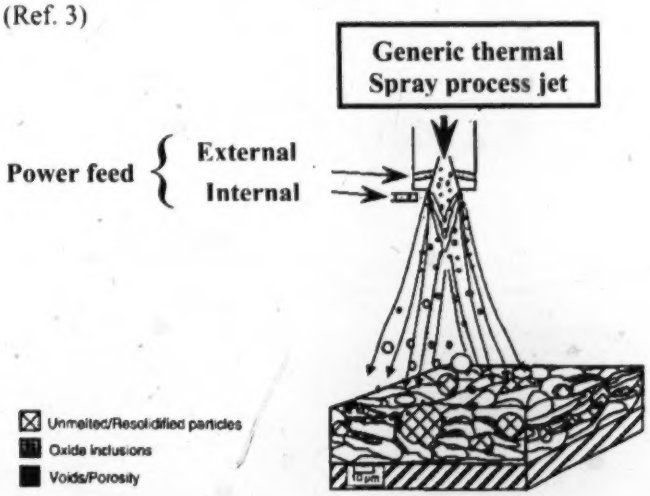

Figure 2-3 Schematic representation of a typical thermal spray powder consolidation process (Ref. 5)

Thermal spray jets heat large numbers (millions) of particles simultaneously, and due to the non-uniform temperature distributions of the spray jets used, and also differing particle sizes, many particles are not heated to the same degree. Some coating particles

may be completely unmelted and can cause porosity or trapped "unmelts" in coatings. The level of these coating defects varies depending on the particular thermal spray process used, the operating conditions selected and the materials being sprayed. Figure 2-4 shows a photomicrograph of HVOF spray 80/20 NiCr alloy coating, which shows the typical lamellar splat structure. The splats and coating layers were built up as each droplet impacted at the substrate. The microstructure in Figure 2-4 includes partially melted particles and dark, oxide "inclusions" that are characteristic of many metallic coatings sprayed in air. (Ref. 3)

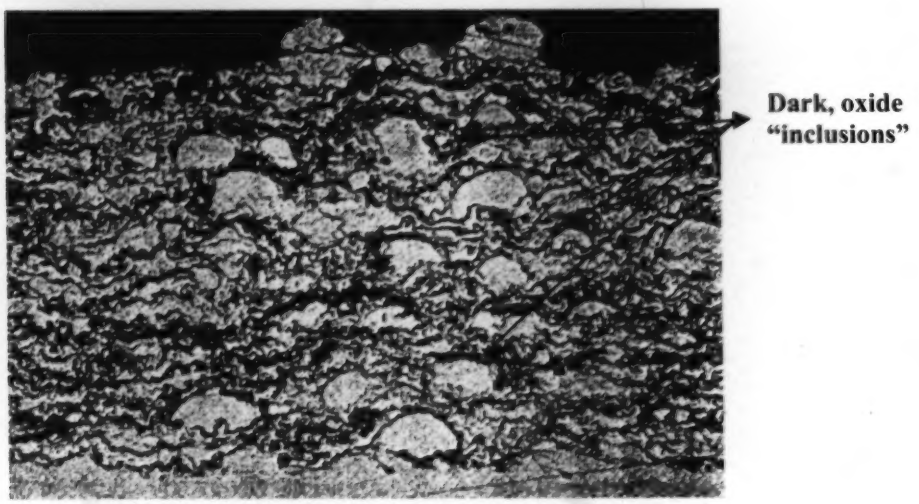

Figure 2-4 Photomicrograph showing the microstructure of a thermally sprayed 80/20 NiCr alloy (Ref. 3)

The key success of HVOF is the extremely High Kinetic Energy that is being produced and transferred between the HVOF unit and the substrate. With both thermal and kinetic energy, the high velocity particles are conformed and adhered on the substrate to form a superior coating with the following characteristics: (Ref. 6)

- High Density coatings produced though HVOF
- High Bond Strengths (in excess of 12,000 Psi)
- Low Porosity (with no interconnecting porosity)
- Metal Working Capabilities
- Essentially Stress Free
- Greater Hardness
- Greater Thickness
- Low Thermal Input (substrate temperature less than 300 degrees F which insures original mechanical properties)
- No Stress Relieving Required

2.1.4 HVOF Coating Materials

Coating particles are typically 50μm in size and they can be used to build up coatings up to 1.52mm (0.060 inch) in thickness. Typically, coatings of 0.076mm (0.0030 inch) to 0.13mm (0.0050 inch) are applied in manufacturing processes and thicker coatings of between 0.25mm (0.010 inch) and 1.52mm (0.060 inch) are applied during repair processes. This project was for remanufacturing crankshafts where the coating thickness for crankshaft journal was 0.51mm (0.020 inch) at the center and 0.38mm (0.015 inch) at the edge. The HVOF spray material used in this project was Metco 4010 iron molybdenum, which is the iron base powder for HVOF process. Metco 4010 is Fe, 30Mo and 2C blended particles. Nominal particle size is –45 +5.5 μm (-325 mesh +5.5 μm). It is developed as an alternative to hard chrome plating, which is recommended to protect against abrasive grains, wear from hard bearing surfaces and fretting. (Ref. 6)

In summary, HVOF is a supersonic process that delivers well over 1400 meter/second (4500 feet/second) of velocity and can exceed bond strengths of 83 MPa (12,000 Psi). It

offers an unlimited range of possibilities to industries with extreme corrosion and wear environments. HVOF coating is emerging as one of the most cost effective ways to repair wear and corrosion.

2.2 Steel Heat Treatment Processes

Heat treatment processes make steel suitable for varies applications by varying the metal properties. This is done by controlling the phase transformations which steels experience in the solid state. Both time and temperature have an important influence on these transformations. Traditionally, most heat treating operations have been carried out in the furnaces with a long heating time for completion, typically one hour per 25mm of thickness for austenitizing or tempering.

Induction heat treatment process of steel combines one of the oldest technologies-steel heat treating with the modern induction heat treatment process. For induction heat treating, which the heating is accomplished by inducted electric currents within metal parts, and heating time can be cut to minutes or even seconds. Induction heating is also attractive for applications involving a surface, such as surface hardening and surface tempering and so on. In these cases, parts can be produced with a special blend of properties that cannot be achieved by other processing methods.

In this project, induction hardened crankshaft journals made of SAE 1040 were remanufactured using a HVOF spray process. Those crankshaft journals with hardened surfaces were heat-treated by the furnace method or by the induction heat-treating

process. Therefore, the following literature review sections discuss the carbon steel, traditional heat treatments, details of induction heat treatments, and other related knowledge.

2.2.1 Carbon Steel

Carbon steels play an important role in the manufacturing industry. Carbon steels, or Carbon-Manganese (C-Mn) steels are alloys of carbon, manganese and iron dominated by the solid state eutectoid reaction at 0.8%C. (Ref. 7) Of all binary alloy systems, the most important is iron and carbon.

Carbon steel is the widest application alloy in industry. The chemical compositions of commercial steels may include as few as two primary elements-iron and carbon or as many as five or more elements. The microstructure, properties and manufacturing process of carbon steel are best understood by referring to the iron-carbon phase diagram. The iron-carbon phase diagram not only can describe any relationships between composition, temperature and microstructures at any balanceable form, but also it can deduce the relationships between properties and composition or between temperature and properties. Therefore, iron-carbon phase diagram is the base of theory for researching on the compositions, the microstructures and properties of steels, and also the heat treatment processes must be setup according to it. (Ref. 8)

The next sections are devoted to the details of the phase diagram for iron-carbon system and the development of several possible microstructures. In addition, the relationships

between heat treatment, microstructure, and mechanical properties are in the following sections.

2.2.1.1 SAE 1040

In this project, the crankshaft journals with induction-hardened surface are made of SAE 1040. SAE 1040 (UNS 10400) is general-purpose medium-carbon fine grain machinery steel. In the production of this grade special controls are used for chemical composition, heating, rolling and surface preparation. These bars are suitable for applications of forging, cold drawing, machining, and induction hardening. Good wear resistance can be obtained by the induction hardening. Table 2-1, Table 2-2 and Table 2-3 as follows are average values for chemical composition, mechanical properties and Forging and Heat Treatment Parameters. (Ref. 9)

Table 2-1 Mechanical Properties for SAE 1040 (Ref. 9)

Tensile strength	87,000 Psi (600 MPa)
Yield strength	52,500 Psi (362 MPa)
Elongation	25 %
Reduction in area	49 %
Brinell hardness	180

Table 2-2 Forging and Heat Treatment Parameters for SAE 1040 (Ref. 9)

Thermal Treatments	**Starts Temperature** (Celsius)	**Finish Temperature** (Celsius)	**Cooling Medium**
Forging	1150 °C Max.	950 °C	-
Annealing	800 °C	830 °C	Surface cool
Normalizing	870 °C	920 °C	Air
Hardening	840 °C	870 °C	Water quench
Hardening	855 °C	885 °C	Oil quench
Tempering	430 °C	700 °C	According to required properties

Table 2-3 Chemical Composition of SAE 1040 (Ref. 9)

	C	Mn	Si	P	S
SAE 1040	0.37 - 0.40	0.60 - 0.90	0.2%	Max. 0.04	Max. 0.05

2.2.2 The Iron-Iron Carbide (Fe-Fe_3C) Phase Diagram

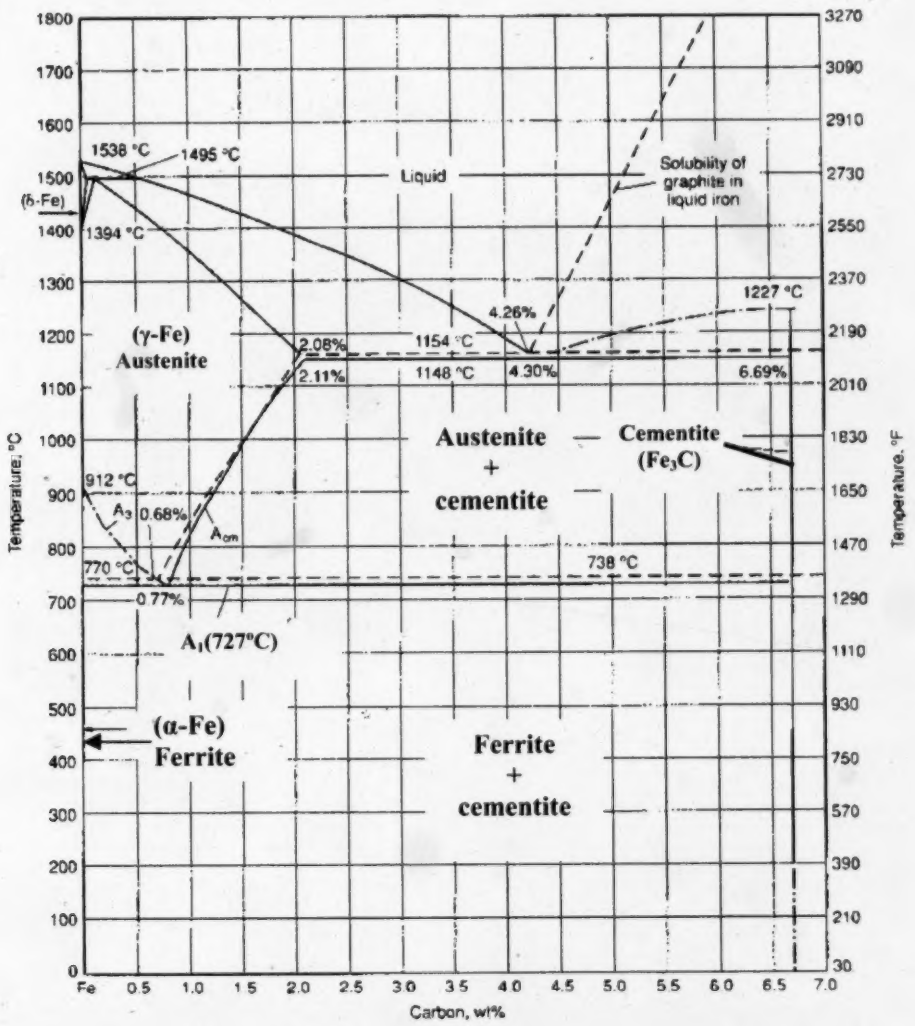

Figure 2-5 The Fe-C equilibrium diagram up to 6.67% wt%. Solid lines indicate Fe-Fe_3C diagram; dashed lines indicate iron-graphite diagram. (Ref. 10)

Iron-Carbon phase diagram is the base of theory for researching on the compositions, the microstructures and properties of steels, and also the heat treatment processes. Figure 2-5 shows the phase diagrams - the stable iron-graphite diagram (dashed lines) and the metastable Fe-Fe_3C diagram. The stable condition usually takes a very long time to develop, especially in the low-temperature and low-carbon range, and therefore the metastable diagram is more practical. (Ref. 14)

The Fe-C diagram shows which phases are at equilibrium for different combinations of carbon concentration and temperature. In Figure 2-5, special names to facilitate the discussion are given to some important boundaries at single-phase fields. (Only the names used to analysis in this project are described as follows) These include: (Ref. 14)

- A_1, the eutectoid temperature, which is the minimum temperature for austenite
- A_3, the lower-temperature boundary of the austenite region at low carbon contents (below 0.77% C), that is, the γ / $\gamma + \alpha$ boundary
- Acm, the counterpart boundary for high carbon contents (over 0.77%), that is, the γ / $\gamma + Fe_3C$ boundary
- Ac_1, the temperature at which austenite begins to form during heating
- Ac_3, the temperature at which transformation of ferrite to austenite is completed during heating
- Ms the temperature at which transformation of austenite to martensite starts during cooling

A portion of the iron-carbon phase diagram is presented in Figure 2-5. The diagram shows the various phase transformations in steel under equilibrium conditions that occur

during heating or cooling. And also it is helpful to explain the properties of steels and predict phase changes in iron-carbon alloys undergoing slowly varying temperature cycles.

The iron-carbon diagram is characterized by three invariant points: a peritectic point at 1439 °C with 0.16 % C, an eutectic point at 1147 °C with 4.3 % C and an eutectoid point at 723 °C with 0.77 % C. (Ref 11) Along the left vertical axis of the phase diagram, it shows that pure iron experiences two changes in crystal structure before it reaches its melting point during heating. At room temperature the stable form is called **ferrite** (or α iron) with BCC crystal structure. Ferrite experiences a polymorphic to FCC **austenite** (or γ iron) when the heating temperature reaches 912 °C (1674 °F). This austenite persists to 1394 °C (2541 °F) until δ ferrite is formed with BCC phase, finally iron melts at 1538 °C (2800 °F).

The composition axis in Figure 2-5 extends only to 6.70 wt% C. Practically, all steels and cast irons have carbon contents less than 6.70 wt% C. For the purpose of understanding the structure of SAE 1040 steel, the regions of interest on the Figure 2-5 are the austenite (γ) to ferrite (α) region at carbon contents less than 0.77 %. In this region, austenite transform to a two-phase structure of ferrite and cementite upon slow cooling, which it follows the left part of iron-carbon phase diagram at temperature below 727 °C. The amount of the ferrite & cementite depends on the carbon content of the steel and the other alloying elements. (Ref. 12) However, in the steel making process, steel is

not formed under equilibrium conditions. The microstructure depends upon both the chemistry of the steel and processing that it undergoes.

In order to understand the effects of heat treatment processes on the microstructure of SAE 1040 steels, the induction hardened crankshaft journal along with the various transformation products after heat treatment processes in these steels must be examined. The microstructure of steel is governed by the kinetics of transformation making the structure dependant on the time and temperatures experienced during process. The effects of time and temperature on the structure of steel are best represented in a continuous cooling transformation (CCT) diagram as shown in Figure 2-6.

2.2.2.1 Continuous Cooling Transformation (CCT)

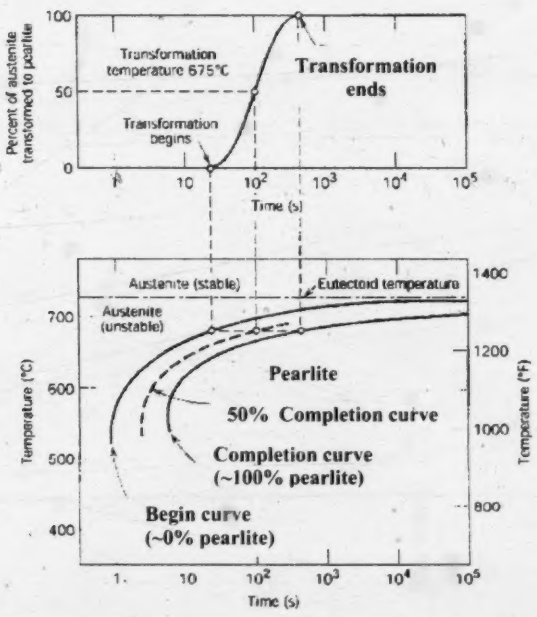

Figure 2-6 Demonstration of how an isothermal transformation diagram (bottom) is generated from percent transformation-versus-logarithm of time measurements (top). (Ref. 13)

In interpreting this diagram, the eutectoid temperature [727°C (1341°F)] is indicated by a horizontal line. At temperatures above the eutectoid temperature for all times, only austenite will exist which is shown in Figure 2-6. The austenite-to-pearlite transformation will occur only if an alloy is supercooled to below the eutectoid temperature. And the time necessary for the transformation to begin and then end depends on the temperature. To the left of the transformation start curve, only austenite will be present, whereas to the right of the finish curve, only pearlite will exist. In between, the austenite is in the process of transforming to pearlite, and thus both micro-constituents will be present. (Ref. 14)

CCT Diagrams is very helpful for setting up parameter for heat-treating process. By conducting the CCT diagram, the proportion of transformation products formed could be determined after the given steel is continuously cooled at different cooling rate to various temperatures intermediate between the austenitizing and the Ms temperature. CCT curves also provide data on the temperatures for each phase transformation, the amount of transformation product obtained for a given cooling rate with time, and the cooling rate necessary to obtain martensite or other microstructures. CCT diagrams can only be read along the curves of different cooling rates. (Ref. 14)

2.2.2.2 Effect of Alloying Elements on Fe-C Phase Diagram

All common substitutional alloying elements in steel could lower or raise eutectoid carbon content and eutectoid temperature of steels in Iron-Carbon phase diagram which are shown in Figure 2-7 and Figure 2-8.

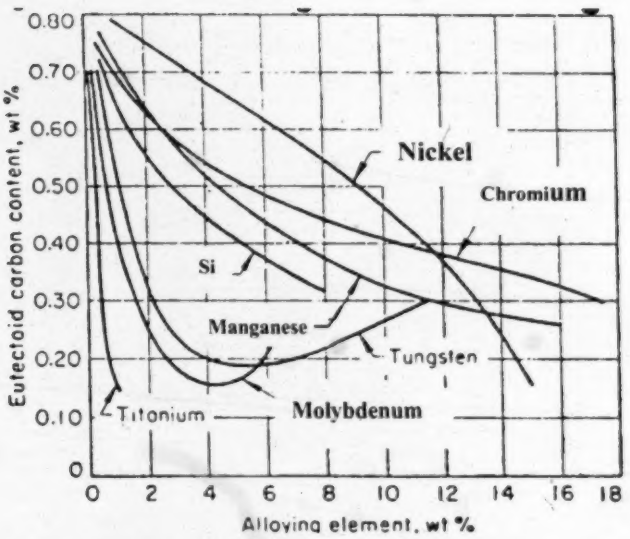

Figure 2-7 The effect of percentage substitutional elements in steel on the carbon content of the eutectoid point (Ref. 15)

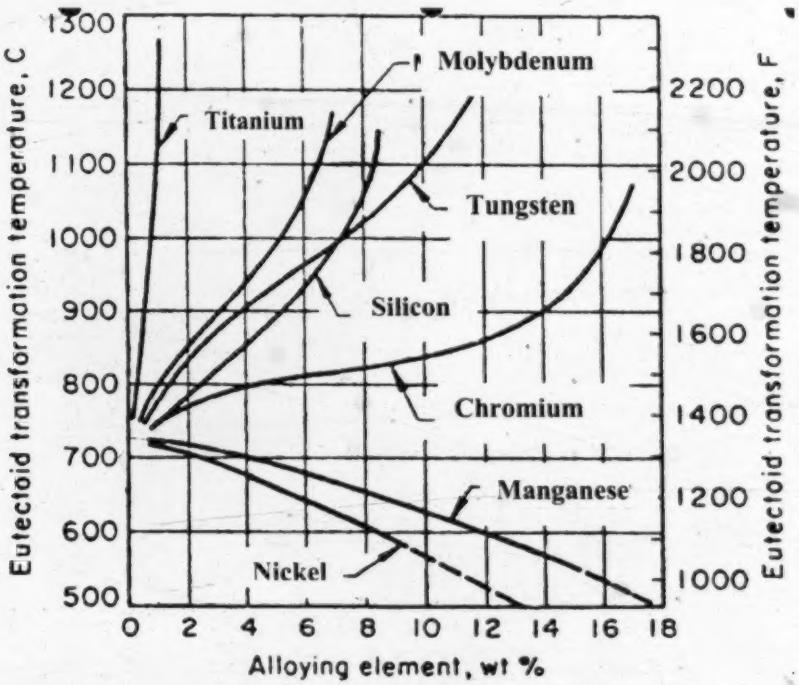

Figure 2-8 The effect of percentage substitutional elements in steel on the temperature of the eutectoid transformation point (Ref. 15)

In this particular case, the material used in this project is SAE 1040. It is plain carbon steel that contains manganese, silicon and other elements-phosphorus and sulphur all grouped in Table 2-4.

Table 2-4 Chemical Composition of SAE 1040 (Ref. 9)

SAE 1040	C	Mn	Si	P	S
	0.37 - 0.40	0.60 - 0.90	0.2%	Max. 0.04	Max. 0.05

In Figure 2-7, it shows manganese and silicon both decrease the eutectoid carbon content. Manganese in SAE 1040 is between 0.6 to 0.9wt%, which could lower the eutectoid carbon content 0.3 wt% roughly. And also 0.2wt% silicon in SAE 1040 steel could reduce the eutectoid carbon content 0.2 wt% approximately from Figure 2-7. Therefore, synthesizing the influence of manganese and silicon on the eutectoid carbon content, the eutectoid carbon content point in Figure 2-5 shift from 0.77 wt% to 0.72 wt% roughly.

In addition, for the eutectoid transformation temperature, there are several methods to determine it. It could figure out from Figure 2-8. Manganese lowers the eutectoid transformation temperature and silicon raises it. And it is also possible to calculate eutectoid and eutectic transformation temperatures using the actual chemical composition of the steel. The following equations will give an approximate critical temperature for hypoeutectoid steel. (Ref. 16)

Equation 2-1

$$A_{C1}(^{\circ}C) = 723 - 20.7(\%Mo) - 16.9(\%Ni) + 29.1(\%Si) - 16.9(\%Cr)$$

$$Standard\ deviation = \pm 11.5\ ^{\circ}C$$

$$A_{C3}(^{\circ}C) = 910 - 203\sqrt{\%C - 15.2(\%Ni) + 44.7(\%Si) + 104(\%V) + 31.5(\%Mo)}$$

$$Standard\ deviation = \pm 11.5\ ^{\circ}C$$

And also in the following table-Table 2-5, it provides approximate critical temperatures for selected steels, measured at heating and cooling rates of 28 °C/h (50 °F/h). For SAE 1040, the eutectoid transformation temperature A_1 is 725 °C (1340 °F) and eutectic transformation temperature A_3 is 795°C (1460 °F), respectively. (Ref. 14)

Table 2-5 Approximate critical temperature for selected carbon and low-alloy steels (Ref. 14)

Critical temperature on heating at 28°C/h (50°F/h)					Critical temperature on cooling at 28°C/h (50°F/h)			
	Ac_1		Ac_3		Ar_1		Ar_3	
Steel	°C	°F	°C	°F	°C	°F	°C	°F
1010	725	1335	875	1610	850	1560	680	1260
1020	725	1335	845	1555	815	1500	680	1260
1030	725	1340	815	1495	790	1450	675	1250
1040	725	1340	795	1460	755	1395	670	1240

Besides the alloy elements in the steel, the heating and cooling rates are often important in the relationship between the heat treatment and the development of microstructure. Most phase transformations require some finite time to go to completion,

The rate of approach to equilibrium for solid systems is slow. True equilibrium structures are rarely achieved unless heating or cooling is carried out at extremely slow and unpractical rates. For other than equilibrium cooling and heating, transformations are shifted to lower or upper temperatures. These phenomena are termed **supercooling** and **superheating,** respectively. The eutectoid temperature A_1 is lowered in supercooling.

And A_1 is raised during superheating. The degree of each depends on the rate of temperature change. The more rapid the cooling or heating rate are, the greater the supercooling or superheating effects, and the more the eutectoid temperature shifts.

In this project, the heating rate by electrical furnace is fast. However, the heating speed by radio-frequency induction furnace is significantly faster, normally the workpiece is heated by induction furnace to austenite temperature in one to two minutes. Therefore, the eutectoid temperature is shifted to 5 to 20 °C (9 to 36 °F) over the equilibrium transformation temperature during heating for SAE 1040. (Ref. 14)

2.2.2.3 Microstructures

The physical properties and mechanical behavior of the steel depend on the microstructures. Many microstructures develop from phase transformations, and the changes that occur between phases upon cooling, such as after heat treatment process. The following sections will discuss the microstructures in detail, and only the microstructures related to this project are included.

- **Ferrite**

Carbon is an interstitial impurity in iron that it forms a solid solution with each of α and δ ferrites, and also with austenite, as indicated by the α, δ, and γ single-phase fields in Figure 2-5. Upon heating, pure iron experiences two changes in crystal structure before it melts. At room temperature the stable form, called α ferrite. Crystal structure for α ferrite is BCC, carbon significantly influences the mechanical properties of ferrite. This particular iron-carbon phase is relatively soft. Mechanically, ferrite is soft and ductile,

but the hardness and tensile strength is low. Figure 2-9 is a photomicrograph of α ferrite. (Ref. 14)

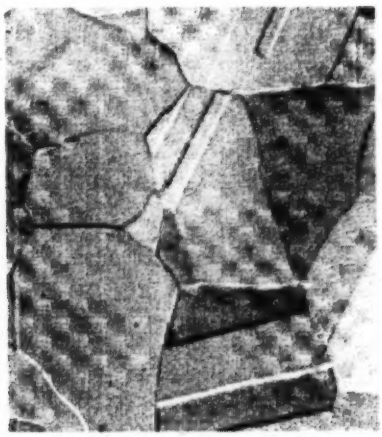

Figure 2-9 Photomicrograph of α Ferrite (90x). (Copyright 1971 by United States Steel Corporation.) (Ref. 14)

- **Austenite**

The austenite, or γ phase of iron, only exist at temperature higher than 727 °C (1341 °F) when alloyed with just carbon. It is unstable below this temperature as indicated in Figure 2-5. In practice, phase transformations involving austenite are very important in the heat treating of steels since austenitizing steel is the key for phase transformation in heat treatment process.

- **Bainite**

Bainite forms in steel when austenite transforms below the acicular ferrite temperature and above the martensite start temperature. Bainite usually exists as only a minor component when present in steel. Its structure is very similar to acicular ferrite by examining optically. But they still have a little difference, that bainite has more elongated microstructure. Bainite is composed of ferrite with over-saturated carbon and

carbide. There are two kinds of bainite - upper bainite and lower bainite. Upper bainite is as "feather" which is formed at upper part of medium temperature zone and lower bainite is needle shape produced at lower part of medium temperature zone. The upper bainite is avoided to be formed since the toughness and strength are quite poor. The expected microstructure is lower bainite with high strength, high hardness, and good toughness also. (Ref. 14)

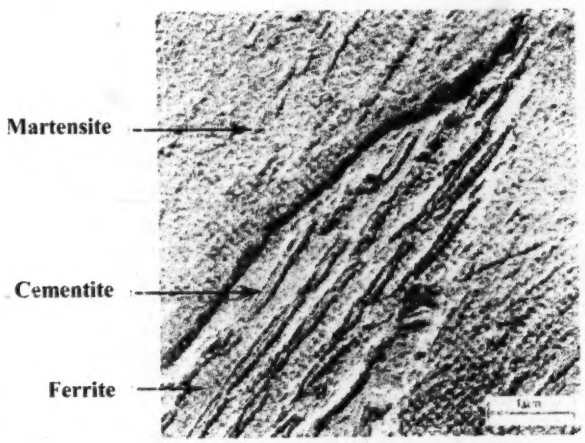

Figure 2-10 Replica transmission electron micrograph showing the structure of bainite. A grain of bainite passes from lower left to upper right-hand corners, which consists of elongated and needle-shaped particles of Fe_3C within a ferrite matrix. The phase surrounding the bainite is martensite. (Ref. 17)

- **Martensite and Retained Austenite**

When austenitized iron-carbon alloys are rapidly cooled (or quenched) to a relatively low temperature Ms, another microstructure or phase called **martensite** is formed. Martensite is a nonequilibrium single-phase structure with BCC crystal structure that the transformation occurs when the quenching rate is rapid enough to prevent carbon diffusion.

Since the martensite results from a diffusionless transformation of austenite, the type of martensitic structure obtained depends on the carbon content of the steel. (Ref. 18) There are two types of martensite - lath martensite and plate martensite. When the carbon content of the steel is lower than about 0.6 wt%, then laths of martensite are observed in the optical microscope which is shown in Figure 2-11, and the quenching temperature is normally higher than 200 °C. As the carbon content is increased to higher than 0.6 wt%, plates of martensite begin to form and quenching temperature is below 200 °C. When the carbon content of steel is between 0.6-1.2 %, the quenched product is the mixtures of lath and plate martensite, as is pointed out in Figure 2-12. As the carbon content of workpiece is higher than 1.2%, the quenched product is totally plate martensite which is shown in Figure 2-13. The lath martensite has good toughness and also high hardness and strength due to low carbon content. However, the plate martensite is very brittle with poor ductility, but very high hardness and strength results from high carbon content. (Ref. 19)

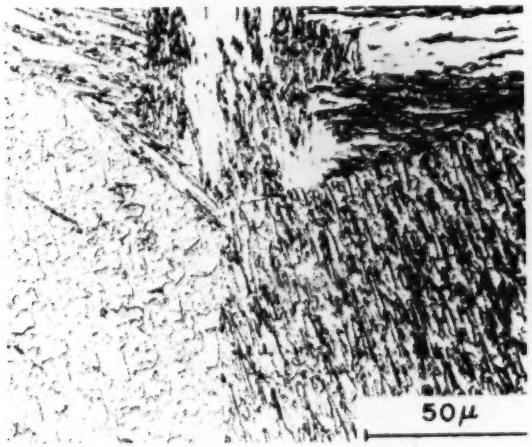

Figure 2-11 Effect of carbon content on the structure of martensite in plain-carbon steels-lath type (Ref. 19)

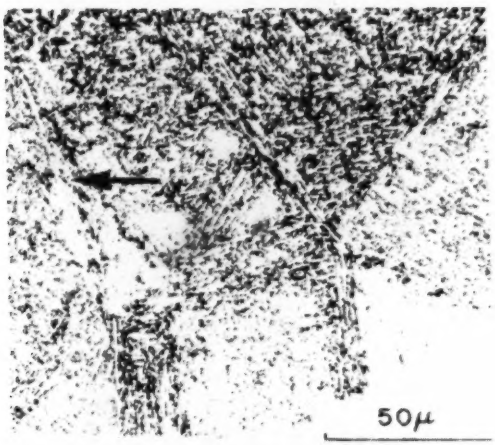

Figure 2-12 Effect of carbon content on the structure of martensite in plain-carbon steels-mixed lath and plate types, arrow points to a plate (Ref. 19)

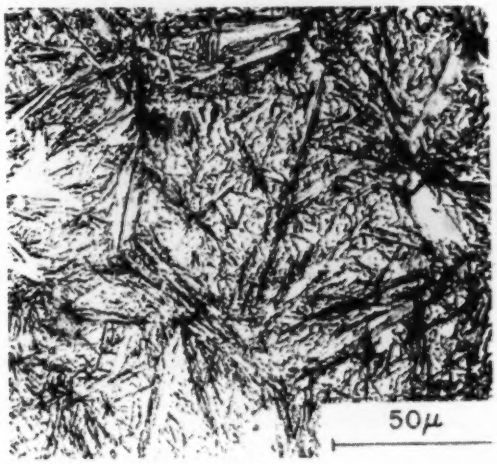

Figure 2-13 Effect of carbon content on the structure of martensite in plain-carbon steels-plate type (Ref. 19)

For retained austenite, as quenched from austenite temperature, some of the austenite did not transform during rapid cooling. As indicted in Figure 2-14, the white phase in the micrograph is retained austenite. (Ref. 19)

Figure 2-14 Photomicrograph showing the martensitic microstructure. The needle-shaped grains are the martensite phase, and the white regions are austenite that failed to transform during the rapid quench. (x 1220) (Photomicrograph courtesy of United States Steel Corporation.) (Ref. 19)

- **Tempered Martensite**

Since martensite in the as-quenched state is very hard and brittle, it cannot be used for most applications. In addition, any internal stresses produced during quenching may have a weakening effect. A heat treatment process – Tempering is applied to improve the ductility and toughness of martensite and also release these internal stresses.

The tempering heat treatment process will be discussed in detail in the following section. The product of tempering is tempered martensite. The tempered martensite composed of the stable ferrite and cementite phases, as indicated on the iron-iron carbide phase diagram-Figure 2-5. The microstructure of tempered martensite consists of extremely small and uniformly dispersed cementite particles embedded within a continuous ferrite matrix. An electron micrograph showing the microstructure of tempered martensite at a very high magnification is presented in Figure 2-15. The tempered martensite has lower hardness and strength, but better ductility compared to martensite. (Ref. 14)

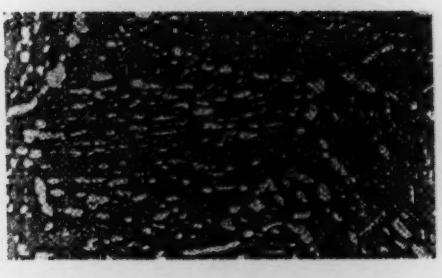

Figure 2-15 Electron micrograph of tempered martensite. Tempering was carried out at 594 ° C (1100° F). The small particles are the cementite phase; the matrix phase is α ferrite. 9300* (Copyright 1971 by United States Steel Corporation.) (Ref. 14)

- **Pearlite**

As shown in Figure 2-5, phase changes upon passing from the γ region into and the $\alpha+Fe_3C$ phase field. Eutectoid steel is slow cooled from austenite region, which its microstructure is composed entirely of the austenite phase initially. As the alloy is cooled down slowly until the temperature is below 727 °C, the pearlite is formed. The microstructure of pearlite is composed of lamellae of the two phases-α and Fe_3C. Figure 2-16 is a photomicrograph of showing the pearlite in the eutectoid steel. The thick light layers are the ferrite phase, and the cementite phase appears as thin lamellae with dark color. Mechanically, pearlite has properties intermediate between the soft, ductile ferrite and the hard, brittle cementite. (Ref. 14)

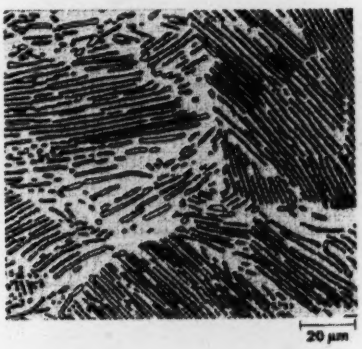

Figure 2-16 Photomicrograph of a eutectoid steel showing the pearlite microstructure consisting of alternating layer of α ferrite (the light phase) and Fe_3C (thin layers most of which appear dark), (500*). (Ref. 20)

2.2.3 Furnace Heat Treatment Processes

Heat treatment processes are very important metal manufacturing processes and they are applied widely in industry. The purpose of heat treatment is to cause desired changes in the metallurgical structure and thus in the properties of metal parts.

Figure 2-5 shows the horizontal line at the eutectoid temperature A_1, which is termed the **lower critical temperature**. Below A_1, all austenite will transform into ferrite and cementite phases under equilibrium conditions. A_3 and Acm lines represent the **upper critical temperature**, for hypoeutectoid and hypereutectoid steels, respectively. Above these two boundaries, only austenite phase exists.

- **QUENCHING**

Quenching is the heat-treating process where the steel is rapidly cooled down from the austenitizing temperature. For most steels including carbon, low-alloy and tool steels, the quenching process produces martensite in the microstructure. The purpose of the quenching process is to achieve high hardness and strength, while minimizing residual stress, distortion and the possibility of cracking. (Ref. 14)

- **TEMPERING**

Tempering is accomplished by heating the martensitic steel to a temperature below the eutectoid for a specified time period, and then cooling at a suitable rate. Normally, tempering is carried out at temperatures between 175 and 705 °C (350 and 1300 °F) with few exceptions. The low-temperature tempering process, which is for releasing internal stresses, is carried at temperatures as low as 200 °C (390 °F). Medium and high temperature tempering is primarily to increase ductility and toughness and reduce

hardness, but is also accompanied with increasing grain size of the matrix. Generally, tempering follows quenching from above the upper critical temperature. Martensite formed by quenching is tempered and softened, forming tempered martensite. Thus the ductility and toughness of the steel are improved and the hardness reduced. (Ref. 14)

- **INTERCRITICAL HEAT TREATMENT**

Intercritical heat treatment is heating the steel to a temperature between A_1 and A_3 (for Hypoeutectoid steel) or between A_1 and Acm (for hypereutectoid steel), and then cooling in still air. This heat-treating process is new compared to other conventional heating treatment. During its heating process, the steel is heated to a temperature between the lower and upper critical temperatures and held for a certain time. The hypereutectoid steel and hypoeutectoid steel revert to austenite and ferrite (except eutectoid steel which is fully austenitized) and the amount of ferrite and austenite formed depends on the heating temperature and carbon content of steel. The cooling process after an intercritical heat treatment normally is air-cooling. The microstructure formed after intercritical heat treatment is typically ferrite, cementite, and retained austenite. For specific steels, the composition of each phase depends on the austenitizing temperature. (Ref. 35)

2.2.4 Induction Heat Treating of Steel

Induction heat treatment of steel combines one of the oldest technologies, (steel heat-treating) with a modern induction heating process. It is one of the most effective heat treatment processes available for a variety of applications including surface hardening, through hardening, tempering and stress relief (low-temperature), annealing and normalizing (high-temperature), weld seam annealing and sintering of powdered metals.

Induction heating provides a means for precise heating of electrically conducting objects. It offers a number of advantages over other heat treatment methods. The most important advantages are short heat treatment times, good repeatability concerning the hardened-layer quality, small or negligible subsequent distortion, and a minimum subsequent product surface oxidation. (Refs. 21, 22 & 23)

2.2.4.1 Principles of Induction Heating

Induction heating is a method of heating electrically conductive materials by the application of a varying magnetic field. In the process, magnetic force lines enter the workpiece, and the varying magnetic field induces an electric potential (voltage), which can then create an electric current. These are so-called eddy currents which produce heat by flowing against the resistance of an imperfect conductor. (Ref. 21)

The basic components of an induction heating system are an induction coil, an alternating-current (AC) power supply, and the workpiece itself. The coil, which may be designed in different shapes depending on the required heating workpieces, is connected to the power supply so that a magnetic field is generated from the high frequency current flow shown in Figure 2-17. The magnitude of the field depends upon the strength of the current and the number of turns in the coil. These induced eddy currents followed Faraday's law of electromagnetic induction which is presented in Equation 2-2. (Ref. 21)

Equation 2-2

$$e = -N\frac{d\phi}{dt}$$

e is the induced voltage

Φ is the time rate of change of the magnetic field

N is the number of turns

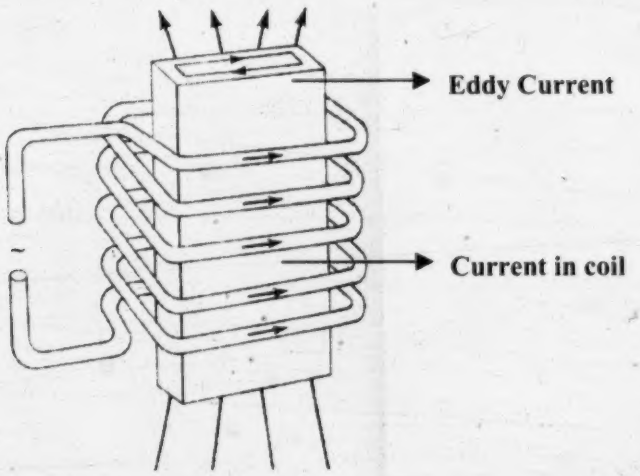

Figure 2-17 Induced eddy current in the specimen is opposite to that in the coil (Ref. 21)

At any moment the direction of the induced current in the workpiece is approximately opposite to the current in the inductor coil. The induced currents generate their own magnetic fields in opposition to the field generated by the coil and thereby prevent the field from penetrating to the center of the object. (Figure 2-17) Therefore, the eddy currents are more concentrated at the surface and decrease in strength toward the center of the object which is shown in Figure 2-18. This phenomenon of the eddy currents generated closer to the surface of a conductor is called the "Skin Effect". The "effective" depth of the current-carrying layers is defined as the "reference depth", which is the distance from the surface of a given material at which the induced field strength and

current are reduced to 37% of their surface values. In Figure 2-18, it shows the current density has dropped by 37% of its surface value at reference depth. The reference depth depends on the frequency of the ac field (f), the electrical resistivity (ρ), and the relative magnetic permeability of the workpiece (μ). The definition of d is shown in Equation 2-3.

Equation 2-3

$$d = 3160\sqrt{\rho/\mu f} \text{ (English units)}$$

$$d = 5000\sqrt{\rho/\mu f} \text{ (Metric units)}$$

Figure 2-19 shows reference depths decrease with higher frequency and increase with higher temperature for various materials at different temperatures. (Refs. 21, 23, 27 & 28)

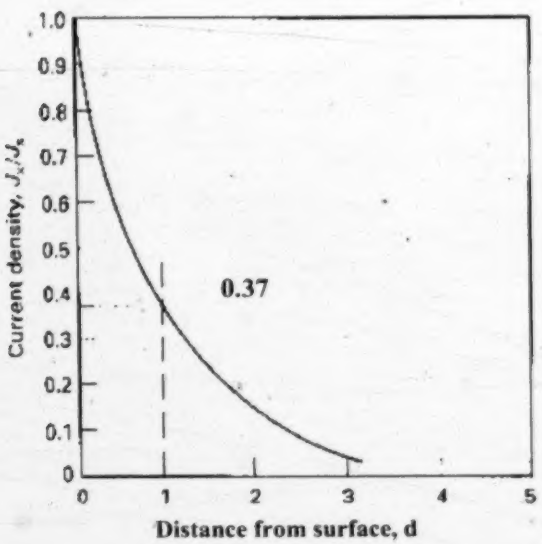

Figure 2-18 Schematics showing current density characteristics. (Ref. 21))

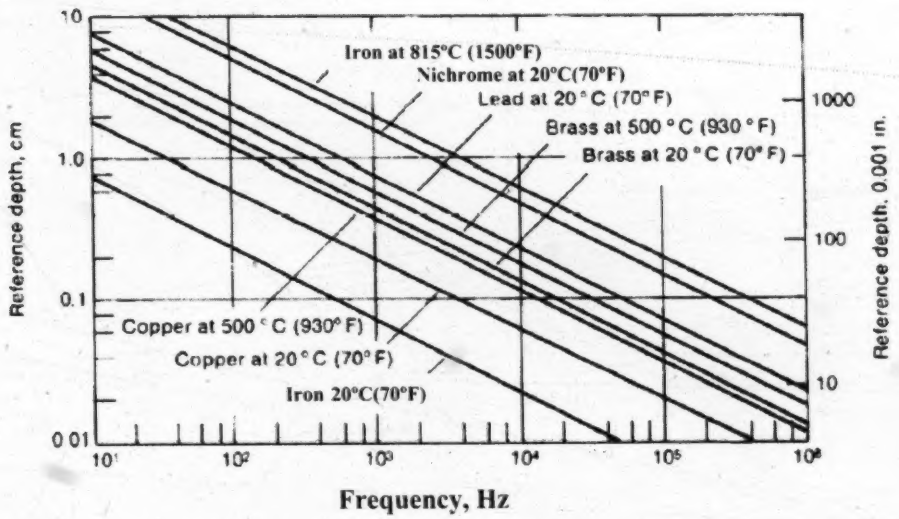
Iron at 815°C (1500°F)
Nichrome at 20°C(70°F)
Lead at 20 ° C (70° F)
Brass at 500 ° C (930 ° F)
Brass at 20 ° C (70° F)
Copper at 500 ° C (930° F)
Copper at 20 ° C (70° F)
Iron 20°C(70°F)
Reference depth, cm
Reference depth, 0.001 in.
Frequency, Hz

Figure 2-19 Reference depth for various materials (Ref. 23)

2.2.4.2 Induction Surface Hardening

A basic characteristic of induction hardening is that eddy current is generated on the surface of the workpiece due to the skin effect. The flow of these currents heats the surface of the workpiece to austenite temperature A_3 (or above temperature Ac_3 for a rapid heating process), which is then quenched by the journal interior to produce a hard martensitic surface layer (This is "self-quenching" by the workpiece itself). The induction heating process is very fast and very reliable. Normally the hardening process also introduces compressive stresses into the surface layers, leading to an improvement in fatigue properties and prevention of crack formation or propagation at the surface. Suitable materials for induction surface hardening usually are plain-carbon or low-alloy steels or cast irons (Ref.21)

2.2.4.3 Induction Tempering and Intercritical Heat Treatments of Steel

The basis for induction tempering and intercritical heat treatments is the same as conventional furnace heat treatments. The major difference is only in replacing long-duration, low-temperature furnace heat treatment; by short-duration, higher-temperature induction heat treatment. In induction heat treatment, the workpiece is mainly cooled down by the conduction of workpiece itself, and partly by the convection and radiation of the surrounding air. Normally, both tempering and intercritical heat treatments are applied on workpieces after induction surface hardening treatment, which could improve the toughness, tensile strength and relieve the residual stress. For induction tempering, there is a limit temperature above which the heating temperature should not be raised. This is the A_1 temperature (or Ac_1 for rapid heating processes), at which carbides start to go back into solution. In addition, the induction tempering process should be called "isothermal tempering treatment" since the tempering temperature is reached in very short time followed by air-cooling. Tempering of hardened steel structures, generally martensite, involves diffusion of carbon atoms to form iron carbide (Fe_3C, or cementite). The tempered products are ferrite and coarse cementite as same as furnace tempering products. (Refs. 24 & 25)

For induction intercritical heat treatment, the heating temperature by induction furnace is between A_1 and A_3. The heating time is very short, even tens of seconds, which produces ferrite and austenite, followed by self-cooling. Eddy currents generated by induction coils are more concentrated on the surface and decrease towards the center of the workpiece. Thus the surface has already been heated above A_1 and transformed to the

ferrite and austenite during heating, but the center part is still at very low temperature and no phase transformation occurs. The cooling process is mainly self-cooled down by the workpiece as induction tempering. The products after intercritical heat treatment are ferrite, cementite and retained austenite, and also a little martensite which do not transform in the furnace intercritical heat treatment due to slower cooling rate. (Ref. 34)

2.3 ASTM Designation C633-01

ASTM Designation C 633-01 is standard test method for determining the adhesion or cohesion strength of thermal spray coatings. The test consists of coating one face of a substrate fixture, adhesive bonding this coating to the face of a loading fixture, and applying a tensile load normal to this assembly of coating and fixtures. It is adapted particularly for testing coatings applied by thermal spray, included the HVOF spray process. The following sections about C 633-01 are all referred to Ref. 26.

2.3.1 Apparatus

The apparatus includes a tensile test machine and a self-aligning device. Tensile test machine is used which could record the maximum load applied before rupture occurs. Self-aligning device (shown in Figure 2-20) is used for applying the tensile load to the assembly of the coating and fixtures, that prevents eccentric load or bending moment on the specimen.

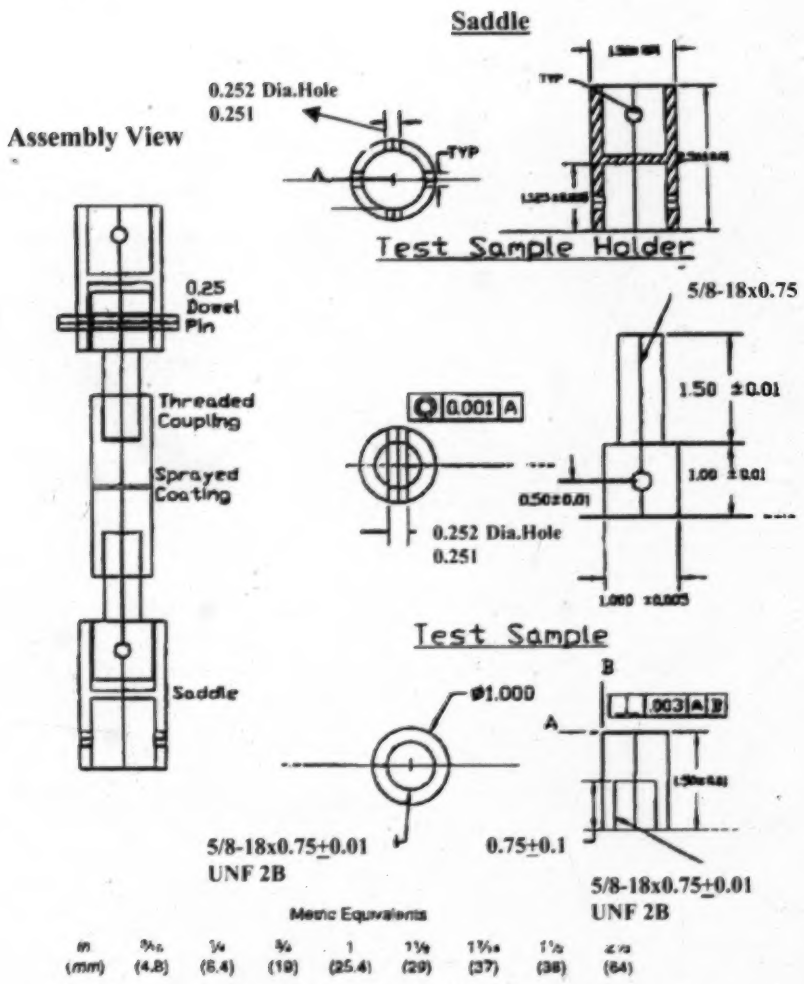

Figure 2-20 Self-Aligning Device and Test Assembly View (Ref. 26)

2.3.2 Materials

Material needed in this tensile test is adhesive bonding agent, which is capable of bonding the coated specimen to the fixture with a tensile strength at least as great as the minimum required adhesion and cohesion strength of the coating. The bonding agent

shall be sufficiently viscous not to penetrate through a 0.38mm (0.015 inch) thickness of the coating.

2.3.3 Test specimen

Test specimens include a substrate fixture with coating applied by HVOF, and a loading fixture. The substrate fixture and loading fixture shall be both constructed of metal, it is usually convenient to make the loading fixture of the same material as the substrate fixture, but the materials for loading fixture is optional. The facing of the loading fixture shall be roughened, cleaned and free of oil and grease mechanically by grit blasting. This facing shall be attached to the surface of the coating by using the adhesive bonding agent. One end of either fixture surface must be square with centerline of thread (shown in Figure 2-21) and the suggested thread size is 12.7mm (0.5 inch), which allows the fixtures attach to the self-aligning loading devices of the tensile test machine. The two fixtures shall be held together parallel and aligned by self-aligning device until the bonding agent is cured or hardened in the oven or at room temperature. The test assembly view is shown in Figure 2-20.

2.3.4 Interpretation of Results

The tensile test set-up according to the ASTM C 633-01 is shown in Figure 2-20. The test machine applies a tensile load to assembly of substrate and loading fixture at a constant rate until rupture and record the maximum load applied when fracture occurs. Low-power microscope with a magnification range up to 100x is suggested for determining the location of failure. It is obvious that the adhesion or cohesion strength

value measured represents the weakest part of the system, where rupture could happen in the coating or at an interface. If the failure is at interface of coating and substrate, the calculated adhesion is the adhesion strength of the coating. If failure is in the bonding agent, then the adhesion strength of the coating is greater than the [illegible]th of the bonding agent. If failure occurs in a combination of these locations in or [illegible]hen, generally no interpretation of the initial cause can be provided.

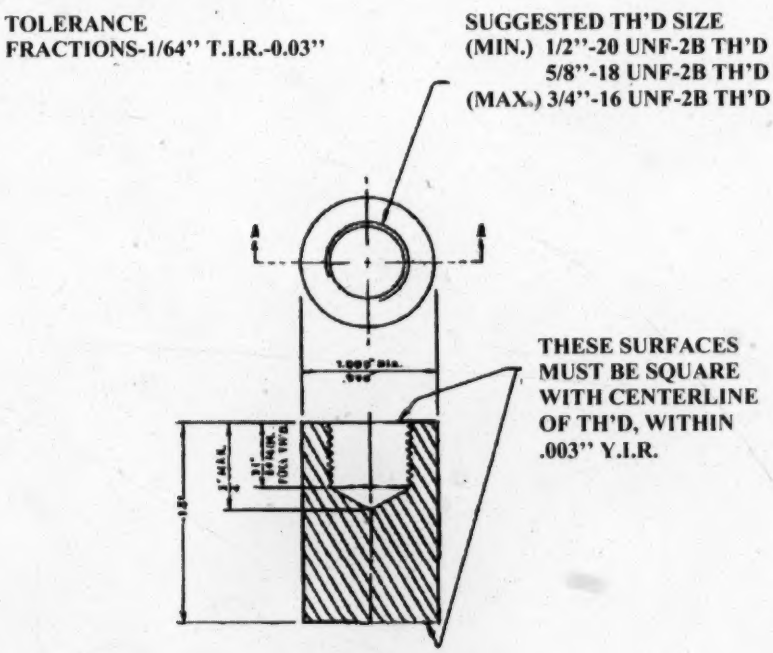
TOLERANCE
FRACTIONS-1/64" T.I.R.-0.03"
SUGGESTED TH'D SIZE
(MIN.) 1/2"-20 UNF-2B TH'D
5/8"-18 UNF-2B TH'D
(MAX.) 3/4"-16 UNF-2B TH'D
THESE SURFACES MUST BE SQUARE WITH CENTERLINE OF TH'D, WITHIN .003" Y.I.R.

SECTION A-A

U.S.	0.003 in.	1/64 in.	31/64 in.	1/2 in.	5/8 in.	
Metric	(0.08 mm)	(0.39 mm)	(12.3 mm)	(12.7 mm)	(15.9 mm)	
U.S.	3/4 in.	0.990 in.	1 in.	1.000 in.	1 ft.	24 in.
Metric	(19 mm)	(25.15 mm)	(25.4 mm)	(25.4 mm)	(0.3 m)	(610 mm)

Figure 2-21 Substrate and Loading Fixture (Ref. 26)

3 Objective

Some crankshafts made of SAE 1040 are used as-machined and can be repaired easily using High Velocity Oxy Fuel (HVOF) power metal overlays. However, other engine manufacturers use the same steel, but induction harden the journal surface. This kind of crankshaft could not be reclaimed by HVOF process due to low bonding strength. The problems occur after cladding and final machining (grinding) of the crankshafts. The overlay fails at the interface with the hardened steel of the crankshaft journal. It is concluded that induction hardening has a deleterious effect on the HVOF repair. The problem appears to be related to the preparation of the induction-hardened surface prior to cladding. Alumina particles are used to blast the surface of a journal to roughen the surface and provide "tooth" for the cladding alloy to bond to the surface. However, due to the high surface hardness of the induction-hardened crankshaft, the grit-blasting process cannot roughen the crankshaft properly as expected. This reduces the "tooth" and leads to failure of the HVOF coatings.

Since the main problem for the HVOF overlay is failure on the induction hardened crankshaft due to the high surface hardness, this study investigated lowering the surface hardness of induction hardened SAE 1040 steel. Then it was reasoned that the conventional surface preparation with alumina particle blasting would be sufficient to provide a good bond with the HVOF deposit. The study objective was to identify short, simple and economic thermal processes for the industry which would mitigate the effects of induction hardening on the application of HVOF overlays for the repair of worn

crankshafts. Finally, the coating's properties for heat-treated crankshaft were evaluated by tensile test and SEM.

4 Experimental Procedure

4.1 Materials and Samples

In this particular project, the crankshaft journal samples obtained from Headhunters Co. were made of SAE 1040 steel (UNS 10400) (Table 2-3). For improving the wear resistance and fatigue strength, the surfaces of crankshaft journals are induction hardened, with a hardened layer about 1.5 mm thick. As in Chapter 2, SAE 1040 is general-purpose medium-carbon fine grain machinery steel. The initial surface hardness of the samples was about 530 Hv. The crankshaft journals were cut into 3.5-inch (88.9mm) diameter with 1-inch (25.4mm) height bulk steels for induction heat treatment experiments. For furnace heat treatment experiments, the samples were cut into small pie-shaped pieces along the crankshaft journals' diameter. (Figure 4-1)

Table 4-1 Chemical Composition of SAE 1040 (Ref. 9)

SAE 1040	C	Mn	Si	P	S
	0.37 - 0.40	0.60 - 0.90	0.2%	Max. 0.04	Max. 0.05

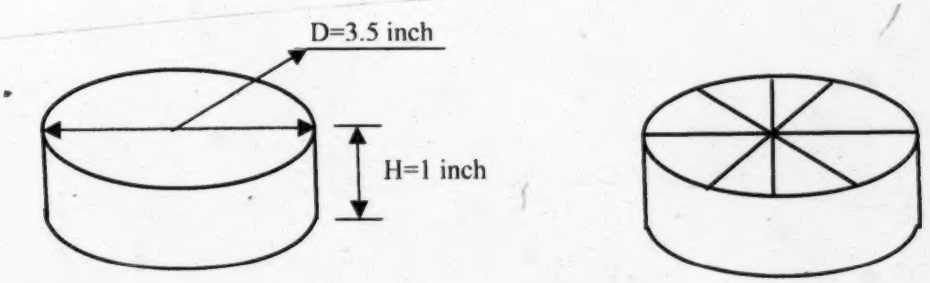

Figure 4-1 Crankshaft Journal Sample and Pie-shaped samples cut from Crankshaft Journal

4.2 *Furnace Heat Treatment*

The short-time furnace heat treatments were applied on the small pie-shaped samples cut from the actual crankshaft journals to reduce surface hardness. The goal for surface hardening is to provide a martensitic layer on specific areas of the workpiece to increase hardness and wear resistance while allowing the remainder of the part to be unaffected by the process. (Refs. 27, 28 & 29) Furnace heat treatments on the crankshaft journal could reduce the surface hardness by tempering the martensitic zone. Two temperature regimes were tried: - a conventional high temperature tempering treatment and a less conventional intercritical heat treatment. The following sections describe the experimental procedures for both furnace heat treatment processes.

4.2.1 Conventional Tempering Heat Treatment

As discussed in Chapter 2, the eutectoid temperature A_1 for SAE 1040 is 725°C (1340°F) and the eutectoid carbon content point shifts from 0.77 wt% in iron-carbon alloys to 0.72 wt%. For conventional high temperature tempering heat treatment, the workpieces are heated to a temperature below A_1 for the purpose of decreasing hardness and increasing toughness. The first group of experiments was run on the small samples cut from the actual crankshaft journals. The samples were heated at 700 °C and 720 °C, respectively. Different holding times in the furnace were tried: - 5 minutes, 10 minutes, 20 minutes and 40 minutes followed by air-cooling. The surface hardness was measured by Vickers Hardness tester, using a 10 kg test load.

A second group of experiments was carried on similar samples using a slightly modified procedure. The samples were preheated at 500 °C, and then heated at 700 °C and 720 °C, respectively. The holding times were still 5 minutes, 10 minutes, 20 minutes and 40 minutes followed by air-cooling. Again, the surface hardness was measured by Vickers Hardness tester, using a 10 kg test load.

Finally, the samples from both groups' were polished to a 0.05 μm finish and etched in 2% Nital, in order to assess the microstructures by microscope.

4.2.2 Intercritical Heat Treatment

For the less conventional intercritical heat treatment, the similar samples were heated at temperatures between A_1 (725 °C) and A_3 (795 °C) for a short time to produce some austenite in the structure as the martensite tempered. In this project, the samples were heated at 740 °C and 750 °C in the furnace for different holding time: - 5 minutes, 10 minutes, 20 minutes and 40 minutes followed by air cooling. The surface hardness was measured by the Vickers Hardness tester, with 10 kg test load. The intercritical heat treatment samples were also polished to a 0.05 μm finish and etched in 2% Nital to assess the microstructures by the microscope.

4.3 Induction Heating Treatment

The furnace heat treatment for both conventional and intercritical process were effective at lowering the surface hardness of crankshaft samples. A similar program using

induction heating in place of the furnace was run to test whether a short time duration process could achieve the same result.

4.3.1 Radio-Frequency Induction Furnace

The induction heating equipment used in this project was a PHILIPS PH1654/01 60 kHz radio-frequency induction furnace. The major purpose of frequency conversion from supply-line frequencies of 60 Hz to radio frequencies of up to 60 kHz and higher is to achieve surface heating at shallow depths in short times and at high power densities. Higher surface-power densities are usually obtained at higher radio frequencies. In this particular case, the output power of the radio-frequency induction furnace was 5 kW. The induction coil was made of 0.3-inch-diameter (7.62mm) copper tube contoured to 6 turns with the coil inside diameter 4.5 inch (114.3mm). The gap length between coils was 0.24 inch (6mm). The following describes the induction heat treatment procedures.

4.3.2 Induction Heat Treatment

The crankshaft journals were heated in the induction furnace coil for different heating times. In the first group of experiments, the samples were heated by the induction furnace for 30 seconds followed by self-cooling and then measurement of the sample surface hardness. This process was repeated twice more, so the total induction heating time was 90 seconds. The hardness data for the three induction heating times were measured using DATALETTY 150 microhardness tester, with a 500g test load and 15 seconds loading time.

In the second group of induction heat treatment experiments, the crankshaft journals were heated for 90 seconds followed by self-cooling. In the third group of experiments, the crankshaft journals were heated for 60 seconds followed by self-cooling. The surface hardness after the induction heating process was measured using the same DATALETTY 150 microhardness tester and test parameters. Finally, the samples which had been induction heated for 60-seconds were polished to a 0.05 μm finish and etched in 2% Nital to assess the microstructures by the microscope and Scanning Electron Microscope (SEM).

4.4 HVOF

The Headhunters Co. was responsible for spraying HVOF coatings for this project. As introduced in Chapter 2, the crankshaft journals were grit blasted by alumina particles before HVOF coating. After roughening the surface, the Metco 4010 iron molybdenum powder was sprayed on using the HVOF process. In order to figure out the differences from the properties of the coating before and after induction heat treatment, the crankshaft journals were coated as required by Headhunters Co. The crankshaft journals were investigated as the follows.

- Crankshaft journals with induction hardened surface were grit blasted to assess the surface roughness before the induction heat treatment.
- Crankshaft journals with induction hardened surface were grit blasted and then coated by HVOF to assess the properties of the coating before the induction heat treatment.

- Crankshaft journals were induction heated for 60-seconds heating time, then grit blasted to assess the surface roughness after induction heat treatment.
- Crankshaft journals were induction heated for 60-seconds heating time, then grit blasted and coated by HVOF to assess the properties of the coating after the induction heat treatment.

Finally, the coated samples after induction heating process were tensile tested according to ASTM C 633-01 standard method to assess the adhesive strength of the coating, which will discuss in Chapter 4.6. In addition, each type of crankshaft samples and initial surface hardened crankshaft samples were polished to a 0.05 μm finish and etched in 2% Nital, then assessed by microscope and SEM analysis.

4.5 Temperature Measurement for Induction Heating Treatment

The success of any induction heat-treating operation depends a great deal on temperature control. In this section, methods of measuring temperature for the induction heating process are discussed. The most common techniques for temperature measuring make use of thermocouples, infrared thermometers and Tempil sticks. Despite the widespread use of each method, several major problems should be considered before a final selection is made. For thermocouples, these include problems of poor workpiece surface condition, eddy current influence, contact resistance, and response time. With an infrared thermometer, emissivity variations are the major cause for concern. For Tempil sticks, even though there are no problems similar to thermocouple and infrared thermometer, the measurement precision is the problem. (Ref. 23)

4.5.1 Thermocouples

Thermocouples provide good accuracy, measurement capability over a very broad temperature range, ruggedness, reliability, and low cost. The method is based on the well-known relationship between a difference in junction temperatures and the resulting voltage (emf). The temperature of the heated junction is determined by measuring the voltage and referring to calibration tables for the particular thermocouple materials. (Ref. 23)

Thermocouples are of two basic types: contact and non-contact (or proximity). In this project, contact thermocouples were used for temperature measurement. There are various types of contact thermocouple arrangements that permit accurate temperature measurements at fast response times. In the experiment, the junctions of two kinds of contact thermocouples are made through the workpiece and then spot-welded on the hard surface of the crankshaft. It could establish the good electrical and thermal contact to produce accurate temperature measurements. However, the junction of contact thermocouples is make of metal, so the eddy current may have influence on the junction itself. The two kinds of thermocouples were used for temperature measurement in the experiment as follows:

- **Temperature measurement by thermocouple without Isolation cover**

The K-type thermocouple is two metal wires without isolation cover. One is a negative pole, and other is a positive pole, they are connected as a junction at the end. The two poles of thermocouple are inserted through a ceramic tube with two individual holes.

Then the junction of the thermocouple is welded by spot welding on the side surface of the sample for temperature measurement. The experiment setup is shown in Figure 4-2.

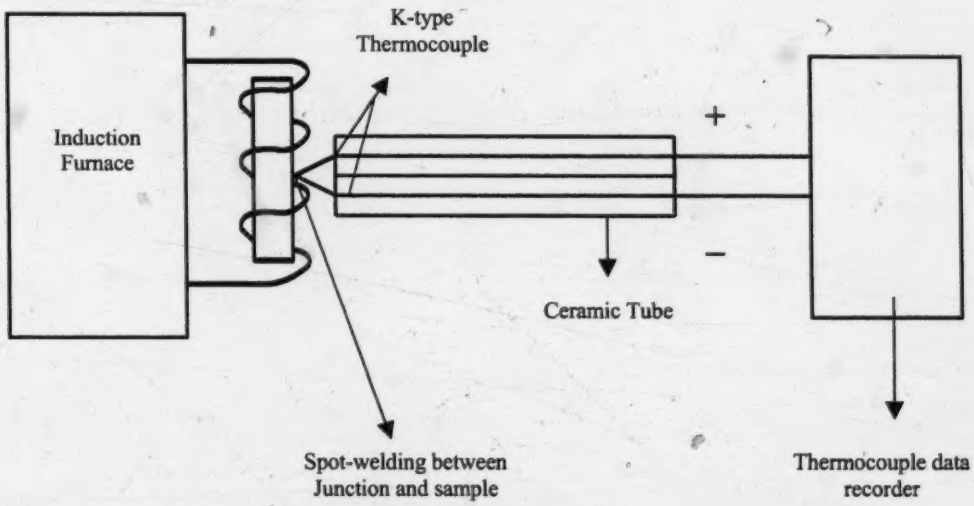

Figure 4-2 Experiment setting up for K-type Thermocouple without Isolation cover

The experiment data for the temperature measurement by K-type thermocouple without isolation cover is plotted in Figure 4-3. As the curve showed, from A to B range, the temperature measured (22°C) is the room temperature before induction heat treatment. From B to C, that is the 60-seconds induction heating treating process. The temperature of the sample's side surface is around 0 °C to 10 °C. That is much lower than the actual temperature since the samples were red heat. Therefore, the eddy current induced by induction heating had a great effect on the thermocouple when it is inserted near to the induction coil to measure the temperature. From C to D, the induction current is stopped, the temperature measured is increased a lot, but it is still much lower than it should be. The reason is because the crankshaft journal was only induction heated to high temperature at the surface due to the eddy current, the center part is still in very low

temperature (about 200 °C), thus the surface of the crankshaft journal is self-cooled down rapidly. In addition, there is the time delay for the thermocouple recorder's responds, the samples had been cooled down for several seconds. Therefore, the temperature measured after D point is the actual surface temperature after several seconds' cooling, which is not the actual induction heating temperature. So the second K-type thermocouple with isolation cover was tried.

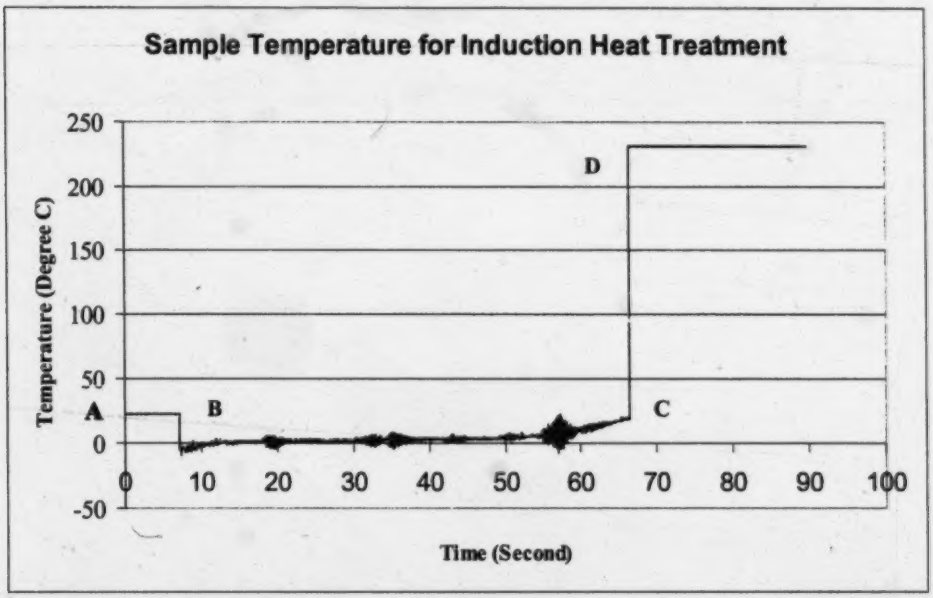

Figure 4-3 Temperature Measurement by K-type Thermocouple without Non-conductive cover

- **Temperature measurement by K-type thermocouple with isolation cover**

Since the metallic junction of K-type thermocouple is heated by the induction coil and thus causes imprecise measurement, the K-type thermocouple with an isolative cover was tried in the this experiment. This kind of thermocouple still has a negative pole and a positive pole, which are covered by an isolative tube. They are connected at the end as a junction. The Figure 4-4 is the K-type thermocouple with isolation cover. For doing the

induction heating temperature measurement, the thermocouple is inserted through an alumina tube for further isolation when it is inserted through the induction coil. The experiment setup is showed in Figure 4-5.

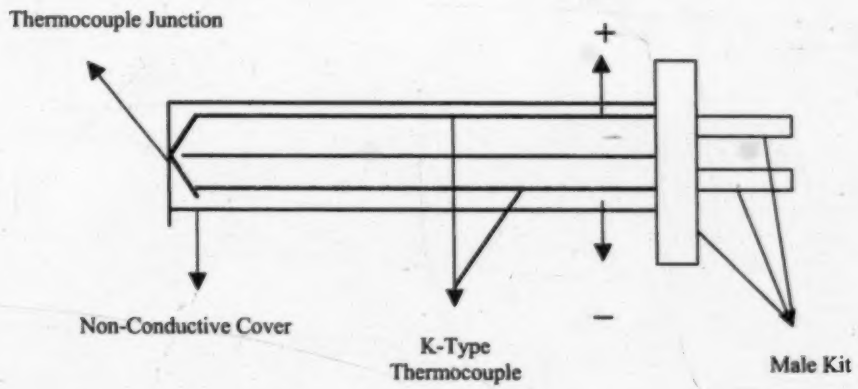

Figure 4-4 K-type Thermocouple with Non-conductive Tube

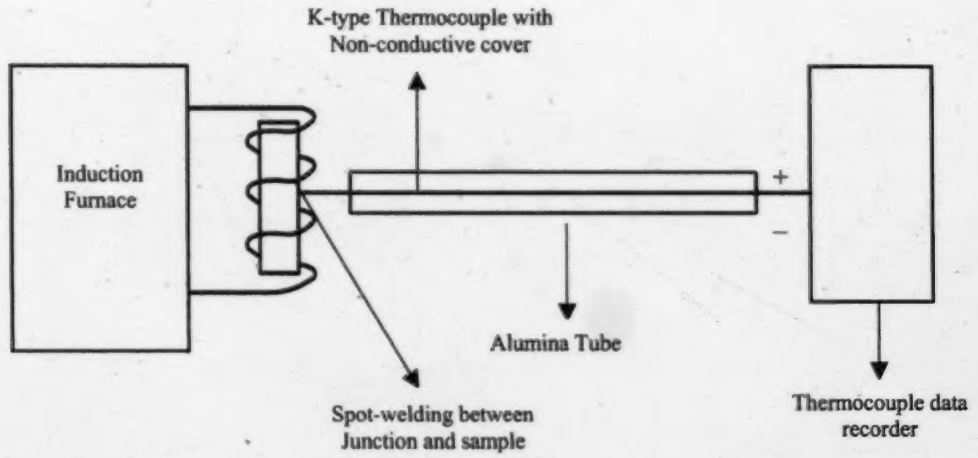

Figure 4-5 Experiment set-up for K-type Thermocouple with Non-conductive Tube

The curve for temperature vs. induction heating time is showed in Figure 4-6:

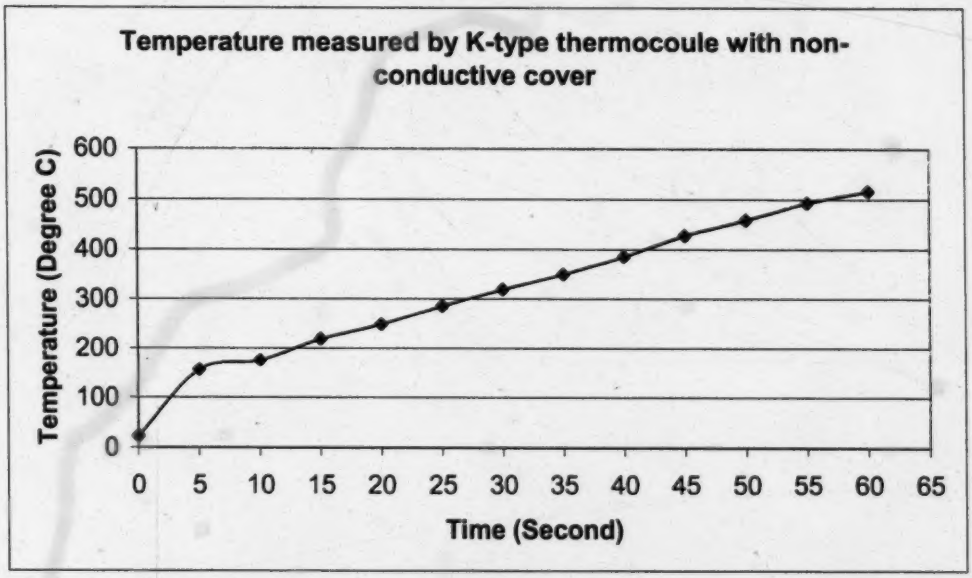

Figure 4-6 Temperature Measurement by K-type Thermocouple without Non-conductive Cover

As the temperature showed above (which was measured by K-type thermocouple with isolative cover), the total induction heating time is 60 seconds, and the highest temperature measured is 515.4 °C, which is still not as high as expected. However, it is not certain whether the induction heating has any effect on K-type thermocouple with isolative cover, which could influence the temperature reading. Therefore, The following temperature-measuring device, the infrared pyrometer was tried for induction heating temperature measurement.

4.5.2 Infrared Pyrometer

The other popular means of rapid temperature measurement in induction heating applications relies on the use of infrared radiation. These devices provide a non-contact

method of measuring the temperatures of hot surfaces during heating. In comparison with thermocouples, infrared pyrometer provides the following advantages: (Ref. 23)

- Because contact is not required, temperatures can be measured without interfering with the heating operation.
- There is no upper theoretical temperature limit for these devices.
- The response during measurement is very fast. The readings are accurate with properly calibrated and maintained instrument.

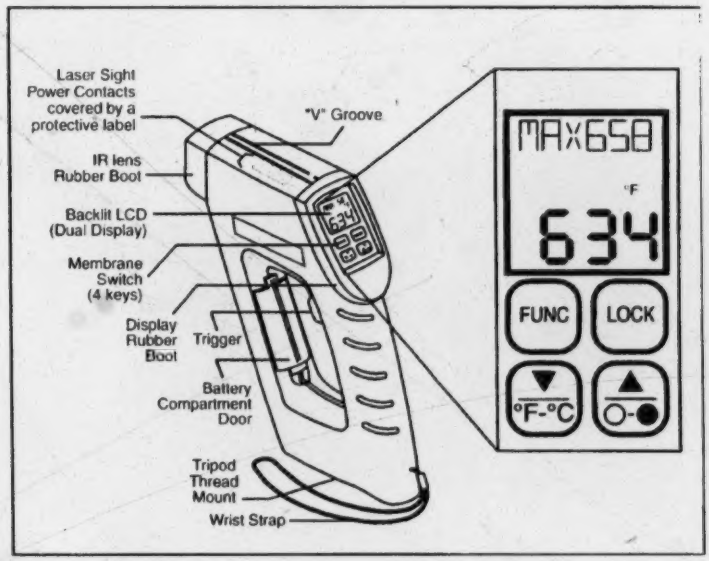

Figure 4-7 OMEGA OS523-3 Infrared Pyrometer (Ref. 30)

In this project, the OMEGA OS523-3 infrared pyrometer (Figure 4-7) was used to measuring the surface temperature for induction heat treatment. For OMEGA OS523-3, the field of View is show in the Figure 4-8. The OMEGA OS523-3 spot diameter is 9mm @ 610mm, but the gap between the induction coils is only 6mm, so the infrared pyrometer could not have enough space to focus through the induction coil gap. Therefore, the recorded temperature of the infrared pyrometer is not the actual

temperature. This conclusion is proved in the practical measurement experiment. The highest readout temperature of infrared pyrometer during the induction heating treatment was 594 °C. The measured result is similar to the thermocouple, so the Tempil sticks were used for measuring the range of induction heating temperature as follows.

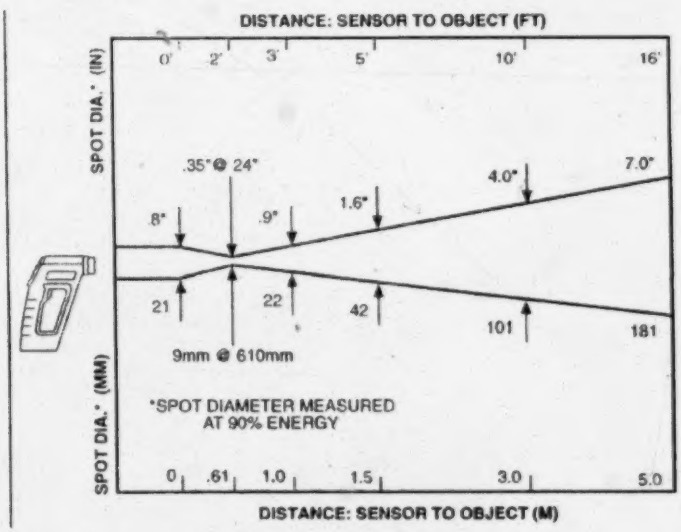

Figure 4-8 Field of View for OMEGA OS523-3 (Ref. 30)

4.5.3 Tempil stick

Since the thermocouple and infrared pyrometer are both unable to properly measure the surface temperature for induction heat treatment, the Tempil sticks were tried for temperature measurement in the experiments.

Tempil stick is a stick of waxy material that melts at a calibrated temperature. It has several advantages for surface temperature detection. It is an inexpensive alternative for temperature measurement, simple without using any gauges or electronics, easy to use anywhere that a hot surface is visible. And it is also reliably accurate since it melts

within ±1% of rated temperature. For the operation, the Tempil stick is marked on the induction heating samples before heating. When the desired temperature has been reached a distinct melt will become evident. But the disadvantage of Tempil stick is that the accurate temperature could not be obtained. Since every Tempil stick has its own melting temperature, the measured temperature by the Tempil stick is only melted or not melted at this temperature. Therefore what the measured results obtained from Tempil stick is a temperature range, not a precise value.

The first group temperature measurement was run. Marking 5 different temperature rating Tempil sticks with different colors on the same bulk of crankshaft journal before the induction heating is carried, the Tempil sticks were 621 °C (the color is light yellow), 649 °C (dark yellow), 677 °C (black), 704 °C (pink) and 804 °C (green). During the 60-seconds of the induction heating, the five different Tempil sticks are melted in the temperature order except the 804 °C Tempil stick. The time respond of the four Tempil sticks melting were recorded.

The second group temperature measurements were carried on the crankshaft journals. The 704 °C Tempil stick was marked on the journals before induction heat treatment. Once this Tempil stick was melted, then the induction-heating furnace was stopped, and the heating time was recorded. The crankshaft journal was cooled down slowly in the air. This experiment fixed the heating temperature below the A_1 temperature (725 °C). It is definitely induction tempering heat treatment. (Ref. 14)

The third group temperature measurement was similar as the second group. The only difference is that the 732 °C Tempil stick was marked on the similar crankshaft journal surface. When this Tempil stick was just melted, the induction heating was stopped, and then the crankshaft journal was cooled by the self-cooling. In this experiment, the heating temperature, (732°C) was between the A_1 (725 °C) and A_3 (795 °C). Therefore, it is for assessing the intercritical induction heat treatment. The second and third group experiments are for analyzing the different results after tempering and intercritical induction heat treatment. (Ref. 35)

4.6 Tensile Test

In order to determine the degree of adhesion (bonding strength) of the HVOF coating to a substrate or the cohesion strength of the coating in tension normal to the surface, the tensile test was run on the crankshaft journals after 60-seconds induction heat treatment with HVOF coating. This determined whether adhesion strength of coating is satisfactory for industry.

ASTM Standard C 633-01, "Standard Test Method for Adhesion or Cohesion Strength of Thermal Spray Coatings" is widely used for evaluating bond strengths of HVOF coating. In this project, the tensile test method used was mainly followed the ASTM C 633-01 standard, but there were made some changes for this particular case. The tensile test was not run on the flat coated surface of the cylinder, which was carried on the curved side surface of the crankshaft journal. Thus the coated surface of substrate fixture was curved, which was different from the standard ASTM C 633-01, the loading fixture was also

changed to curved surface to adapt the attachment with the substrate fixture. Tests were done by applying the coating to the side of a cylindrical test specimen 3.5 inch (88.9 mm) in diameter by 1 inch (25.4 mm) long. The coating surface was bonded to another cylinder which is made of SAE 1045, the geometry is shown in Figure 4-10 and Figure 4-11. The force to pull the cylindrical loading fixture apart was recorded by MTS tensile test machine. The bond strength was calculated by dividing the force by the contact surface area of cylindrical loading fixture. The adhesion or cohesion strength value measured represented the weakest part of the system, whether in the coating or at an interface. A low-power microscope and SEM were used to obtain the images of fracture surface.

4.6.1 Tensile Test Preparation

MTS tensile test machine with a load-indicating device was used for running tensile test in this project. The increasing tensile load is applied on the crosshead which travels at a constant rate of 0.04 mm/sec.

In this project, the self-alignment device allowing reproducible adhesion testing was designed (Figure 4-9) by the Headhunters Co., for quantitative evaluation of cohesion and adhesive fractions on round surfaces. Test specimen was an assembly comprising a substrate fixture glued with a loading fixture. The substrate (the crankshaft journal) was cut along the diameter of the journal into two pieces, and then coated by the HVOF, the cut surface was drilled with a 0.5-inch (12.7 mm) centerline thread for attaching with the holder. The device operated with the samples in the form of half crankshaft journal and a

cylindrical plug with curved end glued on the side of the journal which is shown in Figure 4-13. The plug was made of SAE 1045 25 mm diameter, and its contour is shown in Figure 4-10 and Figure 4-11. And the front facing of the loading fixture was prepared by grit blasting at Headhunters Co. In this test, Master Bond EP15 Glue was used for bonding agent. This bonding agent was cured at 177 °C for one hour. The tensile strength of this bonding agent is 8000 Psi. The Figure 4-12 shows the coated substrate with cylindrical loading fixture were mounted and bonded by bonding agent in a self-aligning device.

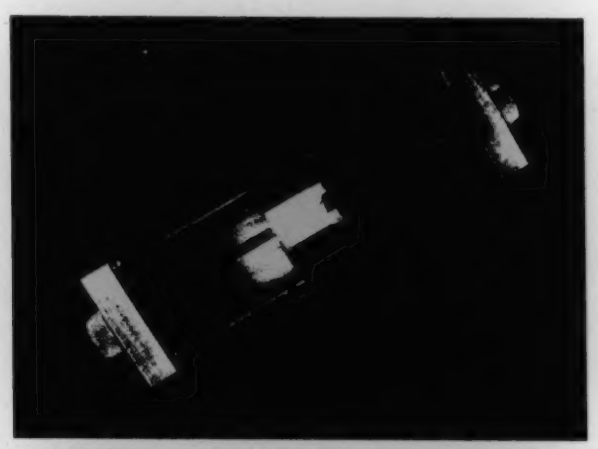

Figure 4-9 Self-Aligning Device for Tensile Test by Headhunters Co.

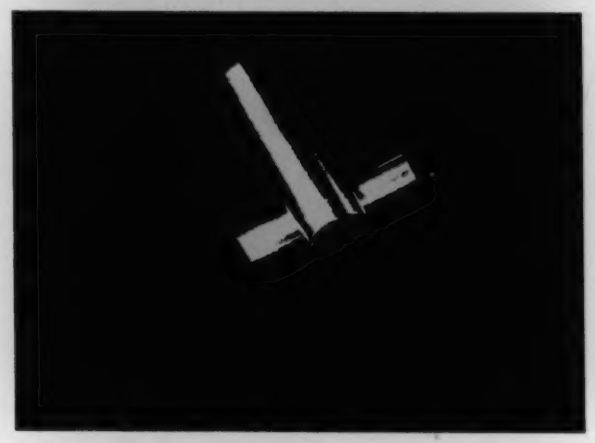

Figure 4-10 The Contour of the Loading Fixture

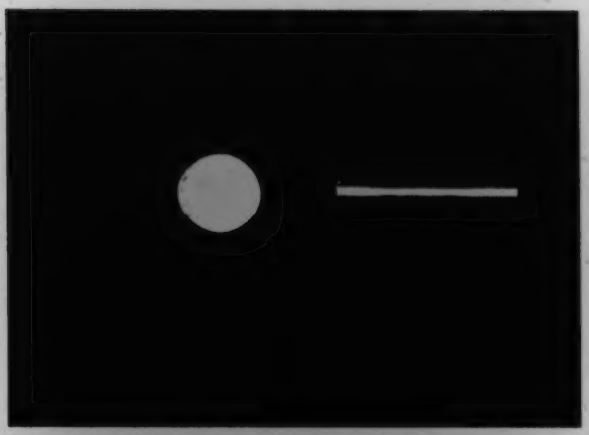

Figure 4-11 The Vertical View for the Loading fixture

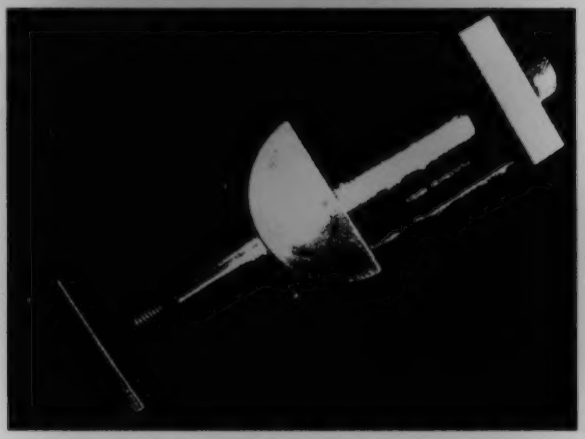

Figure 4-12 Coated substrate with cylindrical loading fixture are mounted in the Alignment Device

4.6.2 Test procedure

- Prepare one substrate fixture-the crankshaft journal after 60-seconds induction heating followed by self-cooling and then grit blasting and spray coating as well.
- Prepare the adhesive bonding agent. The coated crankshaft journal and cleaned loading fixture-small cylinder were then glued together using Master Bond EP15 Glue as it is shown in Figure 4-13 and heated at 177 °C for one hour in the furnace to cure.

- Apply a tensile load to the test specimen at a constant rate of the crosshead travel at 0.04 mm/sec. The crankshaft journal with small cylinder was then pulled apart while the loads applied was monitored and recorded. The load at failure was then noted along with the location of failure. The optical microscope and SEM were used to get image of fracture surfaces for each tensile test.

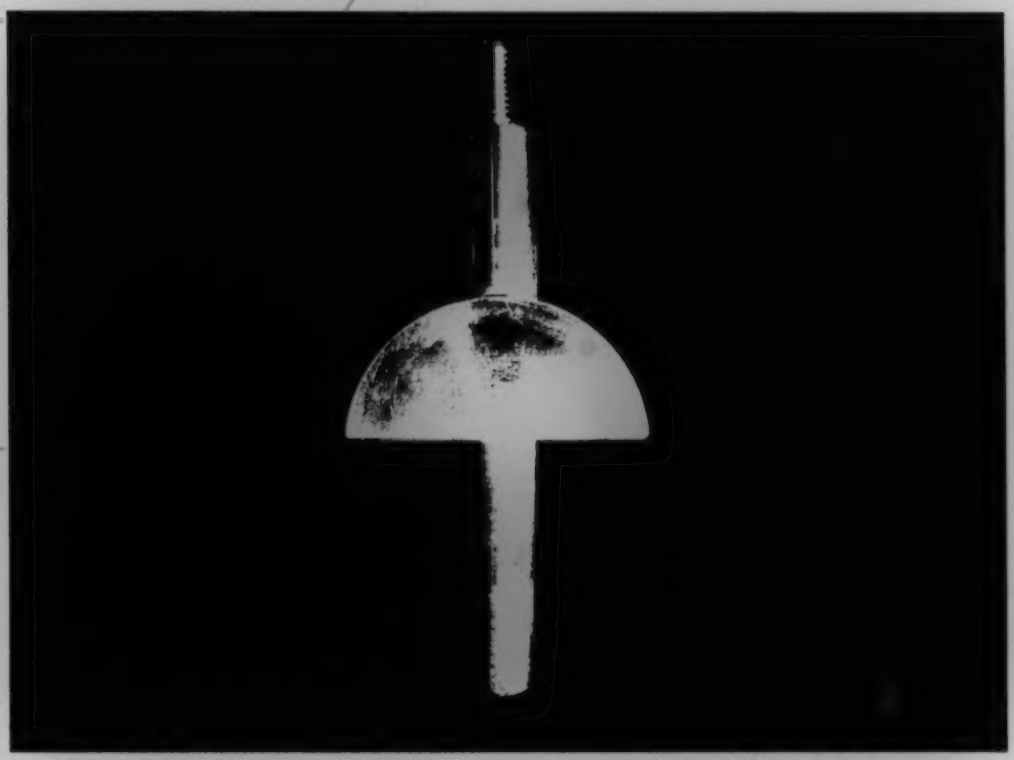

Figure 4-13 The figure for attaching the loading fixture to the coated crankshaft journal

5 Results and Discussions

5.1 Material for Initial Crankshaft Journal

5.1.1 Microstructure

The initial crankshaft journal is made of SAE 1040 with 1.5mm-thick induction hardened layer. As mentioned in Chapter 2, the induction hardened surface is produced by heating the SAE 1040 to the temperature above A_3 by induction furnace, most of the heat is produced on the surface of crankshaft due to the "skin effect". The surface microstructure is totally austenitized during heating and then it cooled very rapidly, the austenite in the steel transforming to martensite when the Ms temperature is reached. No holding time below Ms is required for such a reaction. This is because martensite is formed by a diffusionless reaction involving shear of the FCC lattice into a distorted bct lattice. At fast cooling rates, the formation of ferrite is suppressed, and martensite a less densely packed body-centered tetragonal (bct) structure than austenite, is formed. (Ref. 22) Figure 5-1 is the scanning electron microphotograph of the initial crankshaft surface, and Figure 5-2 is optical image. The etchant for both images is 2% Nital. This image confirms that the microstructure is typically the lath-martensite.

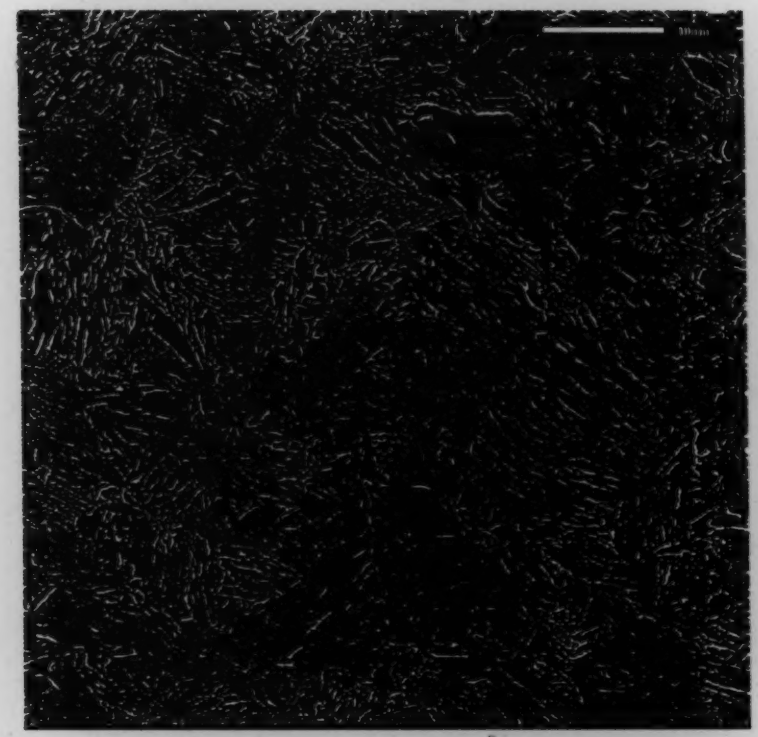

Figure 5-1 Microstructure for Initial Crankshaft surface by SEM (x1500)

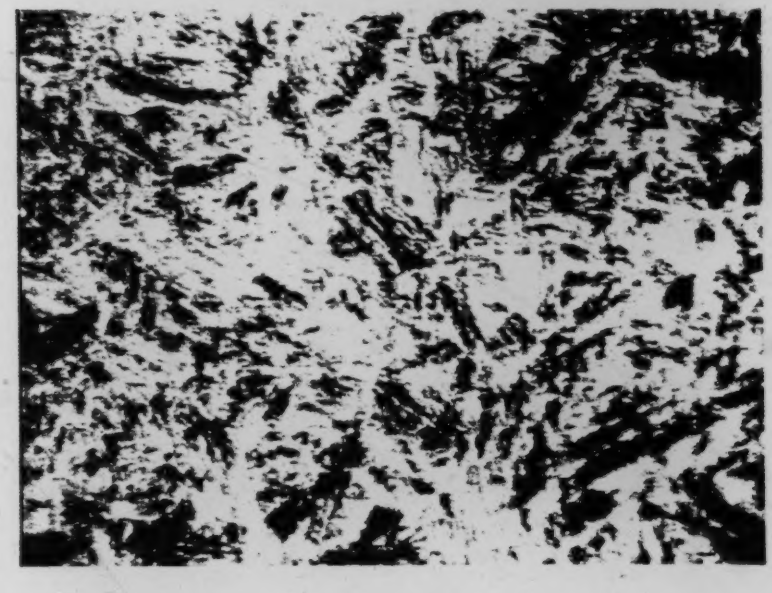

Figure 5-2 Microstructure for Initial Crankshaft surface by Microscope (x 630)

5.1.2 Hardenability

When the crankshaft journal is quenched into a water or oil bath, the surface layers are lath-martensite. However, in the center of the crankshaft, which must be cooled by conduction of heat through the outer layers and which thus cools more slowly, the Ms temperature will not be reached prior to transformation of some of the austenite to pearlite or bainite. In this project, the crankshafts supplied by Headhunters Co. have a 1.5 mm induction hardened layer. And surface hardness is about 530 Hv by Vickers hardness tester. This compares with the center hardness of about 280 Hv. The high hardness surface of the crankshaft is difficult for surface preparation for HVOF. Grit blasting cannot roughen the surface as required, due to the high hardness.

5.2 Hardness Analysis after Conventional Furnace Heat Treatment

For the conventional furnace heat treatment, four groups experiments were run. The surfaces of the specimens for microhardness measurements were polished and measurements made using a 10g load in a Vickers hardness tester. The data are shown in the following tables.

	Microhardness (Hv)					Average Hardness (Hv10)
5 Min.	345	333	333	329	338	336±6
10 Min.	297	285	297	289	302	294±7
20 Min.	263	264	285	285	258	271±13
40 Min.	274	274	285	258	258	270±12

Table 5-1 Surface Hardness of Samples after Furnace Tempering at 700 °C (Initial surface hardness is 518 Hv)

	Microhardness (Hv)					Average Hardness (Hv)
5 Min.	297	289	297	289	285	291±5
10 Min.	297	274	285	274	285	283±10
20 Min.	274	279	263	245	258	264±13
40 Min.	249	264	249	254	254	254±6

Table 5-2 Surface Hardness of Samples after Furnace Tempering at 720 °C (Initial surface hardness is 514 Hv)

	Microhardness (Hv)					Average Hardness (Hv)
5 Min.	302	297	309	302	294	301±6
10 Min.	254	264	254	258	268	260±6
20 Min.	249	254	258	249	249	252±4
40 Min.	236	232	249	249	236	240±8

Table 5-3 Surface Hardness of Samples after Furnace Tempering at 700 °C with preheating at 500 °C (Initial surface hardness is 525 Hv)

	Microhardness (Hv)					Average Hardness (Hv)
5 Min.	264	258	268	264	258	262±4
10 Min.	258	249	254	264	249	255±6
20 Min.	232	232	236	249	228	235±8
40 Min.	232	228	236	232	232	232±3

Table 5-4 Surface Hardness of Samples after Furnace Tempering at 720 °C with preheating at 500 °C (Initial surface hardness is 518 Hv)

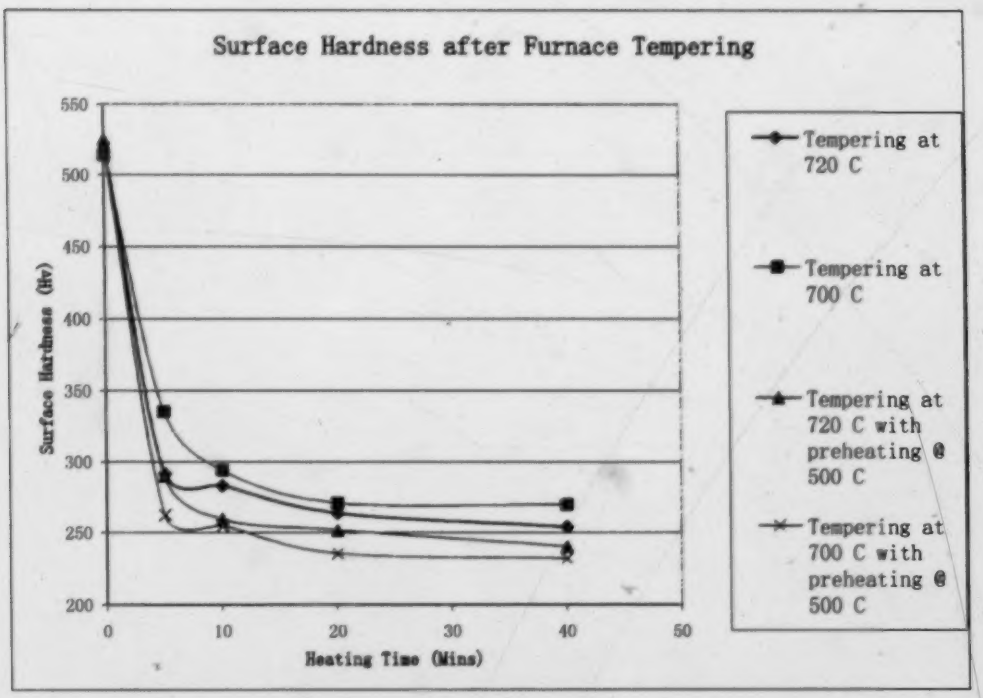

Figure 5-3 Surface Hardness after Conventional Furnace Heat Treatment

As the data show, the crankshafts samples were heated at temperature 700 °C and 720 °C, which was just below A_1 temperature. After 5 min, 10 min, 20 min and 40 min heating time followed by the air-cooling, the surface hardness is reduced greatly after high temperature tempering process when it is compared to the initial hardness. This is because the martensite in the crankshaft surface layer transform to tempered martensite after high temperature tempering. Tempering process involves heating hardened steel to some temperature below eutectoid temperature in order to decrease hardness and increase toughness. From the data, it is concluded that the higher the heating temperature is, the lower the surface hardness is expected. After 5 minutes heating followed by air-cooling, the surface hardness is effectively reduced for the four different tempering processes. As shown in Figure 5-3, a longer heating time could lower surface hardness at the same

tempering temperature than the shorter heating time. Alternatively, a higher tempering temperature cause more hardness reduction at the same heating time than a lower tempering temperature. The difference in the hardness is, however, small.

From the Fe-C phase diagram Figure 2-5, the most stable microstructure below A_1 temperature is the mixture of ferrite and cementite. The other kinds of microstructures' free energy are higher than this mixed microstructure, thus they all tend to transform to ferrite and coarse cementite. However, this transformation is processed by diffusion of the atoms. Therefore, quenched steel has to be heated to the temperature below A_1 and hold for a certain time, allowing the phase transformation to be processed by the stronger diffusion of atoms. In the high temperature tempering process where the heating temperature is just below A_1 for 20-40 ^{o}C, the product of this tempering process is tempered martensite. Tempered martensite is composed of ferrite and coarse cementite, which has very good toughness and low hardness. The initial surface microstructure is the brittle martensite with high hardness, after the tempering process, it is transformed to ferrite and cementite. Therefore, the crankshaft journal samples surface hardness is reduced greatly after conventional furnace heat treatment. And the higher tempering temperature is, the more hardness is reduced.

In addition, the furnace heat treatment with preheating could lower hardness more than the same heating temperature without preheating. That is because preheating is also a medium-temperature tempering process, which could help the α phase recovery and recrystalization. As the tempering time becomes longer, the temperature of the carbide

transformation becomes lower. And when the tempering time is increased and still below A_1, the only difference between preheating and without it is the grain size and configuration.

Since the holding time and preheating did not cause big difference for the hardness value, only one microstructure image from each temperature for the conventional furnace heat treatment is shown. Figure 5-4 and Figure 5-5 show the microstructure after tempering at 720 °C and 700 °C for 10 minutes. Both microstructures are typically tempered martensite - the small and uniformly dispersed cementite particles (dark particles) embedded within a continuous ferrite matrix (bright area). The cementite is curved shape in the ferrite matrix. The microstructures after tempering also show the reasons for the surface hardness reduction.

From the above experiment data and analysis, it concludes that the conventional but short-term heat treatment is effective in reducing the surface hardness for SAE 1040 induction hardened steel.

Figure 5-4 Microstructure for tempering at 720 °C (x 630)

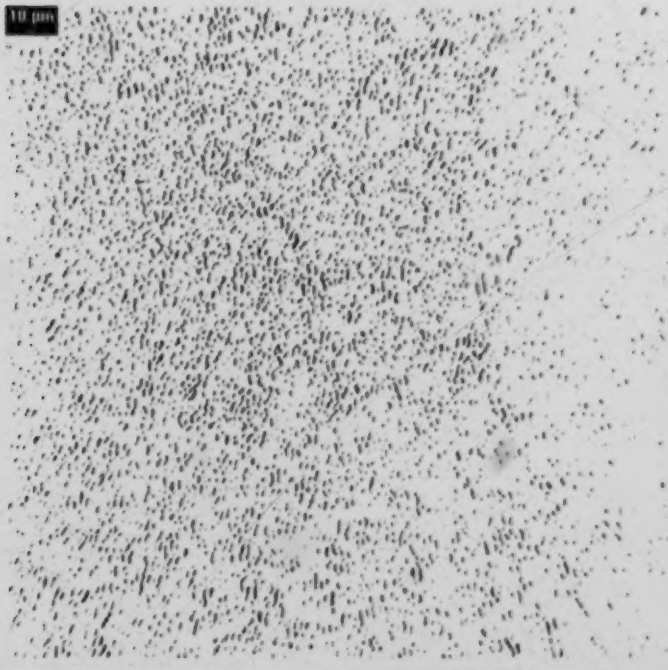

Figure 5-5 Microstructure for tempering at 700 °C (x 630)

5.3 Hardness Analysis after Intercritical Furnace Heat Treatment

Since the conventional heat treatment worked well on reducing surface hardness for induction hardened SAE 1040 steel, the intercritical heat treatment was also carried out on the small pie-shaped samples cut from actual crankshaft journals. The heating temperatures 740 °C and 750 °C are just between A_1 and A_3. After different heating time- 5 minutes, 10 minutes, 20 minutes and 40 minutes, the samples were cooled down slowly in air. The surfaces of the specimens for microhardness measurements were polished and measurements made using 10 g load in a Vickers hardness tester. The surface hardness is shown in Table 5-5 and Table 5-6. In addition, the curves for surface hardness vs. different heating time are plotted in Figure 5-6.

	Microhardness (Hv)					Average Hardness (Hv)
5 Min.	302	309	302	302	294	302±5
10 Min.	274	274	279	264	274	273±5
20 Min.	268	268	264	258	268	265±4
40 Min.	254	254	264	249	258	256±6

Table 5-5 Surface Hardness of Samples after Furnace Tempering at 740 °C (Initial surface hardness is 518 Hv)

	Microhardness (Hv)					Average Hardness (Hv)
5 Min.	297	264	274	285	268	278±13
10 Min.	245	258	254	254	258	254±5
20 Min.	236	254	264	245	264	253±12
40 Min.	249	254	249	249	236	247±7

Table 5-6 Surface Hardness of Samples after Furnace Tempering at 750 °C (Initial surface hardness is 515 Hv)

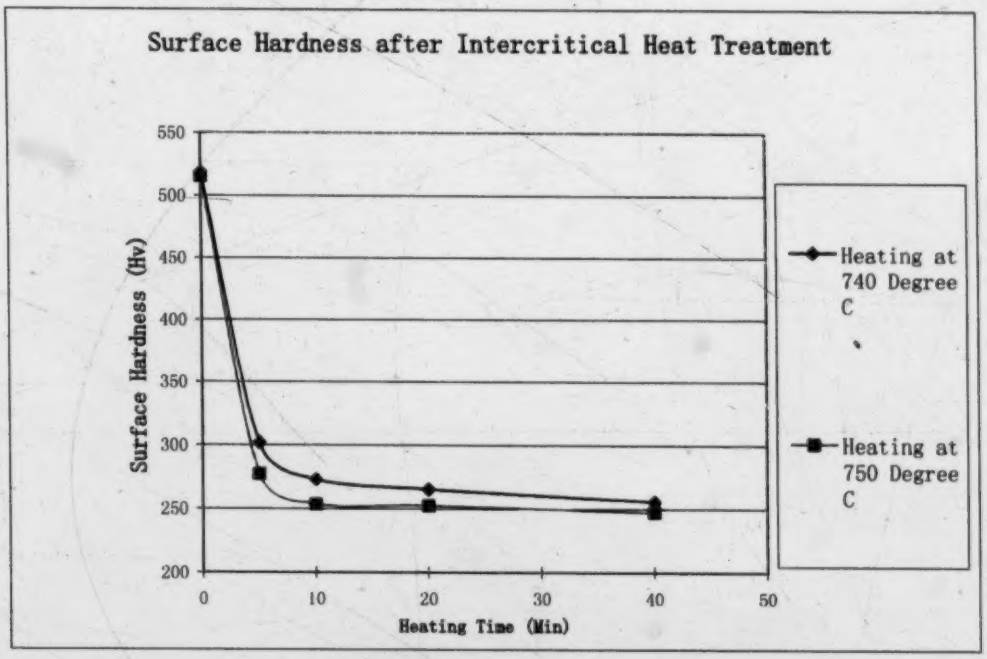

Figure 5-6 Surface Hardness after Intercritical Furnace Heat Treatment

As the experiments show, the surface hardness of the samples is reduced significantly after intercritical heat treatment. The hardness reduction was even more than that achieved by conventional tempering heat treatment with the same holding time. After a 5-minute intercritical tempering, the surface hardness for both heating temperatures is reduced to about 300 Hv. A longer heating time at the same temperature caused a little more hardness reduction. The higher temperature of 750 °C also lowered surface hardness slightly more than the lower temperature of 740 °C for same heating time. Since the preheating before furnace tempering heat treatment did not cause much difference in surface hardness reduction, the intercritical heat treatment with preheating was not assessed.

SAE 1040 is hypoeutectoid steel since the carbon content is 0.4%. The intercritical heat treatment is performed in ferrite + austenite ($\alpha + \gamma$) temperature region between the lower transformation temperature (A_1) and the upper transformation temperature (A_3). For SAE 1040, the transformation temperature A_1 and A_3 are 725°C (1340°F) and 795 °C (1460 °F), respectively. When an intercritical heat treatment at the heating temperature slightly above the A_1 temperature is applied on the samples, the amount of reformed austenite and ferrite are produced followed the Fe-C phase diagram shown in Figure 2-5. The amount of reformed austenite is regarded as a function of temperature between A_1 and A_3. In the particular case, the amount of reformed austenite is approximately 40%, and 60% ferrite. (Ref. 31) Then the samples are cooled down slowly in air.

Figure 5-7 and Figure 5-8 present the optical micrographs showing microstructural evolution after the intercritical heat treatment. The samples were polished to a 0.05 μm finish and etched in 2% Nital. The initial microstructure of crankshaft journal surface is typical martensite, as shown in Figure 5-2. The microstructure after intercritical heat treatment is a composite structure of ferrite (white matrix), cementite (dark phase) and retained austenite. During heating at an intercritical temperature, the carbides dissolve, and the austenite phase forms on the grain boundaries and lath boundaries where the carbon content increases rapidly, and also ferrite forms. In the subsequent cooling, some austenite phase transforms to ferrite and cementite. (Ref. 32, 33) The composite structure of ferrite and cementite is seen in Figure 5-7 and Figure 5-8. The higher intercritical heating temperature made a little coarser grain size. As compared to the microstructures with conventional furnace heat treatment (shown in Figure 5-4 and Figure 5-5), it

indicates that the intercritical heat treatment process makes the microstructure coarser than the conventional heat treatment. For the retained austenite, during the heating, this intercritical heat treatment process promotes the softening of the martensite and the precipitation of finely distributed austenite along the martensite interlath boundaries and prior austenite grain boundaries. After the air-cooling, this austenite remains untransformed and it is known that this accounts for the high toughness and low hardness of this steel. (Ref. 34 & 35)

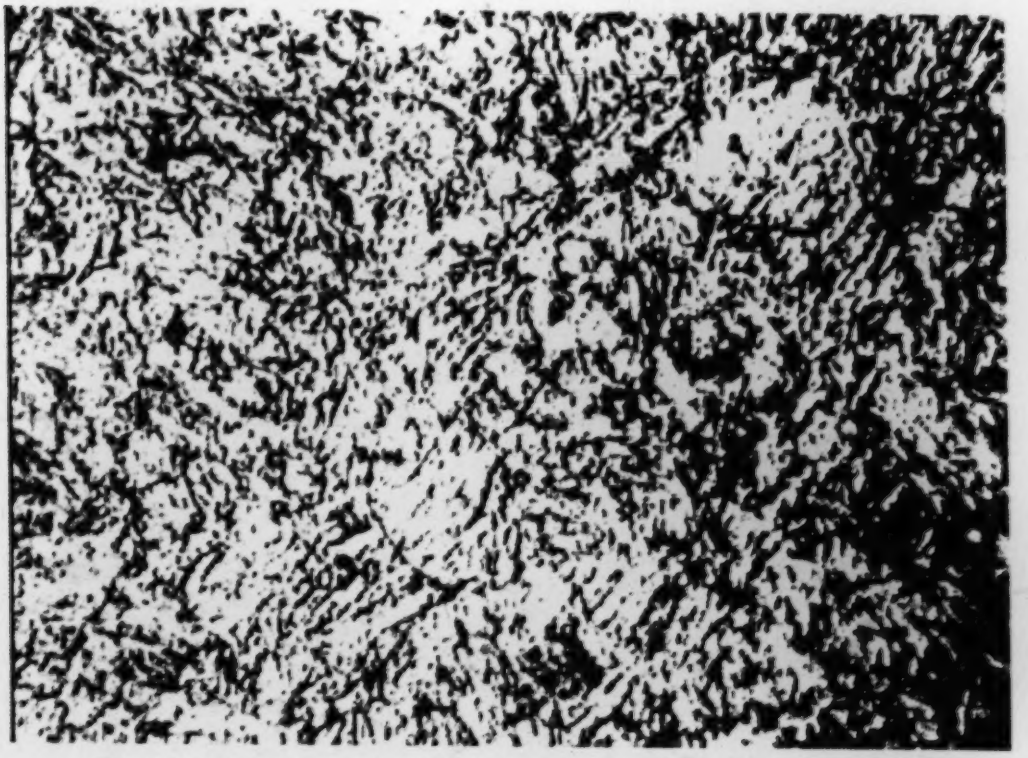

Figure 5-7 Microstructure for Intercritical Heat Treatment @ 740 °C-5 min. (x 630)

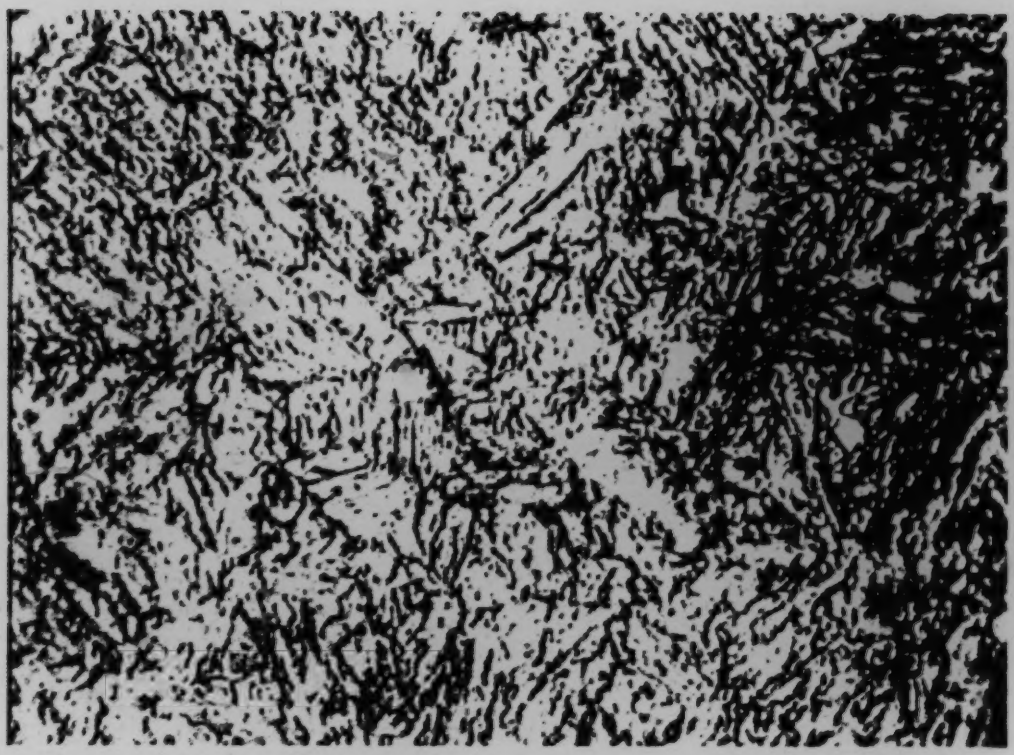

Figure 5-8 Microstructure for Intercritical Heat Treatment @ 750 °C-5 min. (x 630)

As the analysis above, the intercritical heat treatment could lower the surface hardness of induction-hardened steel by forming some retained austenite, ferrite and cementite. It is very effective to lower the surface hardness.

5.4 Hardness Analysis after Induction Heat Treatment

Give that furnace heat treatment is effective to lower the surface hardness of the crankshaft journal, a similar program using induction heating in place of the furnace was carried out on the actual crankshaft journals. The objectives was to identify shorter time induction heat process to lower surface hardness.

5.4.1 Reference Depth for Induction Heat Treatment

In this project, the crankshaft journal samples were induction heated by 60 kHz high-frequency induction furnace. The objective of the induction heat treatment was to lowering the hardness of the 1.5mm-thick induction hardened layer on the crankshaft journal. Thus the reference depth produced by this induction furnace must cover the 1.5mm-thick induction hardened layer. The reference depth depends on the frequency of the ac field (f), the electrical resistivity (ρ), and the relative magnetic permeability of the workpiece (μ), which was discussed in Chapter 2. The calculation follows Equation 2-3 shown below:

$$d = 3160\sqrt{\rho/\mu f} \quad \text{(English units)}$$
$$d = 5000\sqrt{\rho/\mu f} \quad \text{(Metric units)}$$

The magnetic permeability μ of a non-magnetic workpiece is equivalent to that of air and is assigned a value of 1. The electrical resistivity of metals ρ is a function of temperature (Figure 5-9). As shown in figure below, the electrical resistivity of carbon steel-SAE 1040 is 0.92 μΩ · m at 704 °C, 1.0 μΩ · m at 732 °C. After calculating, the reference depth for induction surface heat treatment at 704°C and 732 °C are 1.97 mm and 2.053 mm, respectively. Therefore, the 60 kHz high-frequency induction furnace used in the project is the practical equipment for doing the induction heat treatment on 1.5 mm-thick induction hardened layer.

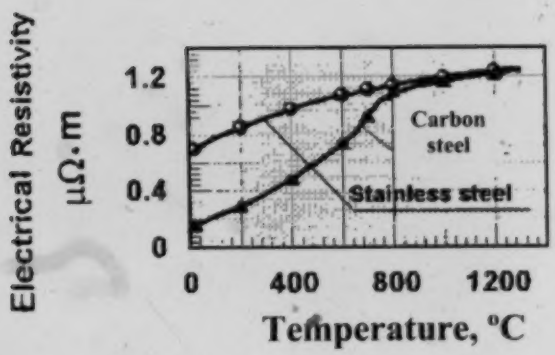

Figure 5-9 Electrical Resistivity of Steels (Ref. 36)

5.4.2 Experimental Data for Induction Heat Treatment

Five groups of induction heat treatment experiments were run. The crankshaft journal was heated inside the induction coil by the induction furnace for different heating time. In first group of experiments, the samples were heated by three 30-seconds induction heating cycles followed by self-cooling as it was described in Section 4.3.2. The surface hardness of the sample was measured by microhardness tester after each heating cycle. The results are shown in Table 5-7.

	Microhardness (Hv)					Average Hardness (Hv)
1st 30-sec	464	464	473	450	464	463±8
2nd 30-sec	366	342	373	373	401	371±21
3rd 30-sec.	285	279	285	289	279	283±4

Table 5-7 Microhardness data for the first group induction heat treatment (Initial surface hardness is 515 Hv)

In second group of experiments, the crankshaft journals were heated by the induction furnace for 90 seconds followed by self-cooling. In third group of experiments, the crankshaft journals were heated by the induction furnace for 60 seconds followed by self-

cooling. The surface hardness after different induction heating process were recorded. The experiments data are shown in Table 5-8.

	Microhardness (Hv)					Average Hardness (Hv)
90-sec.	228.5	227.7	224.9	232.1	216.1	222±11
	208.4	203.5	231.7	235.4	215.7	
60-sec.	297.2	295.6	303.1	286.8	295.6	290±10
	287.3	279.4	301	287.3	270.9	

Table 5-8 Microhardness data for second and third group experiments (Initial surface hardness is 518 Hv)

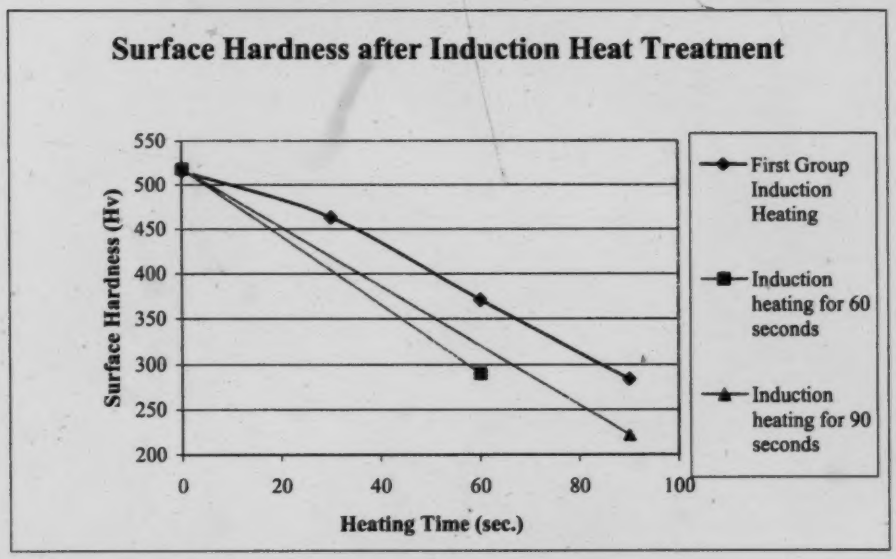

Figure 5-10 Surface Hardness after Induction Heat Treatment

As the experiments show, the surface hardness of induction-hardened steel could be lowered by short-time induction heat treatment. After three different induction heating processes, the surface hardness were all reduced to below 300 Hv. The first group induction process takes much longer time than the other two induction heating processes, due to triple times for the cooling process. For the second group induction process, the surface hardness of the crankshaft is reduced to 222.4 Hv which is even lower than the hardness in the center part. As compared with the third group induction process, the surface hardness after 60-seconds of induction heating was a little lower than 300 Hv.

From economic and practical considerations, the second group induction heating process take less time than the third induction heating treatment, but still lower the surface hardness significantly. Therefore, the 60-seconds induction heating process followed by self-cooling is the most effective and economic induction heating process for reducing surface hardness of SAE 1040 induction hardened steel.

In the fourth group of experiments, the different temperature Tempil sticks were put on the crankshaft journals before induction heating. There are 621 °C (the color is light yellow), 649 °C (dark yellow), 677 °C (black), 704 °C (pink) and 804 °C (white). The induction heating time was still 60 seconds by radio frequency induction furnace. During the induction heating process, the Tempil sticks are melted from the lower to higher temperature except the 804 °C Tempil stick. The time corresponding to the melted temperatures were recorded as follows:

Tempil sticks	Induction Heating Time (Seconds)
621 °C	35
649 °C	47
677 °C	52
704 °C	55
804 °C	Not Melted

In order to get the different influences on surface hardness from the induction tempering heat treatment and induction intercritical heat treatment, the following experiments (fifth group experiments) were run. The 704 °C and 732 °C Tempil sticks were marked on the

two similar crankshaft journals before induction heat treatment. During induction heating process, when these two Tempil sticks were just melted, then the induction furnace was turned off, and the heating time were recorded. The samples were cooled down slowly in air. After cooling down, the hardness for both crankshaft journals were measured. The experiments data show in Table 5-9. Since the first sample was heated at 704 °C which fixed the heating temperature below the A_1 temperature, it is definitely an induction tempering heat treatment. After 55-seconds of induction heating, the surface temperature reached 704 °C. The second sample is heated by induction furnace with 732 °C Tempil stick marked, which is between A_1 and A_3. After 67 seconds induction heating, the surface temperature is reached 732 °C. Therefore, it is for assessing the intercritical induction heat treatment.

	Microhardness (Hv)					Average Hardness (Hv)
Heating @ 704 °C	326.9	363.5	313.3	325.7	341.5	342±18
	351.6	365.7	324.5	352.3	356.4	
Heating @ 732 °C	309.8	271.6	294.8	275.1	291.0	290±12
	280.5	282.6	294.6	297.2	298.3	

Table 5-9 Microhardness data for second and third group experiments

These two groups of experiments show, the induction tempering heat treatment is effective to lower the surface hardness of crankshaft journal, the hardness was reduced to 342.14 Hv after 55-seconds induction heating. However, the intercritical induction heat treatment obtained much more hardness reduction than the induction tempering, even though with only a few more seconds induction heating. From the 55-seconds, 60-seconds and 67-seconds induction heat treatment on the crankshaft journals, the hardness reduction is increased as the induction heating time is longer. And it is obvious that intercritical heat treatment works much better than conventional induction heat treatment.

Among these three induction heating processes, the 55-seconds has much higher surface hardness than the other two processes, the 60-seconds and 67-seconds induction heating process obtained very similar hardness results. From the hardness analysis, the 60-seconds induction heating process may be the intercritical heating treatment, but it still need to be further proved from the microstructure assessment.

5.4.3 Microstructure Analysis after Induction Heat Treatment

As the experimental data show in Section 5.4.1, among the first three groups' experiments, the surface hardness after 60-seconds induction heating is reduced greatly, and also it is proved to be the most economic and effective heating process. Then the crankshaft samples after 60-seconds induction heating treatment are polished to a 0.05 μm finish and etched in 2% Nital. Figure 5-11 presents the SEM micrographs showing microstructural evolution after the 60-seconds induction heat process.

Since the induction heating temperature for 60-seconds induction process could not be measured exactly, it could not decide whether the actual temperature is higher than eutectoid point (A_1), this heating process may be induction tempering or induction intercritical heat treatment. The initial microstructure of crankshaft journal surface is typical martensite as shown in Figure 5-1 and Figure 5-2. In Figure 5-11, it could be seen clearly that the surface microstructure is composed of ferrite (dark matrix) and cementite (bright phase), some retain austenite and a very little martensite.

Since there is some martensite phase formed after 60-seconds induction heat treatment, this heating process should be intercritical induction heat treatment. The martensite was formed from the austenite phase after intercritical annealing due to rapid cooling rate. During induction heating at temperature between A_1 and A_3, the carbides dissolve, and austenite and ferrite phase forms on the surface due to "skin effect", but the center part of the journal is still "cool" (about 200 °C). In the subsequent cooling process, even though the crankshaft is cooled down in air, the cooling process is mainly self-cooled through conduction, and a little convection and radiation through air. The cooling rate more rapid than in furnace heat treatment since the furnace heat treatment is cooled only depend on convection and radiation in air. Therefore, a little austenite phase transforms to martensite because the enrichment of alloying elements, mainly carbon, is enough to have a sufficient hardenability for the martensite transformation under this rapid cooling rate. (Refs. 32 & 33) However, the amount of the martensite is quite little, thus it cannot influence surface hardness a lot.

For the retained austenite, during heating, the intercritical heat treatment process promotes the softening of the martensite and the precipitation of finely distributed austenite along the martensite interlath boundaries and prior austenite grain boundaries. After cooling, some austenite remains untransformed and it is known that this accounts for the high toughness and low hardness of the steel. (Ref. 34 & 35) Thus the surface hardness is reduced significantly due to ferrite, cementite and retained austenite produced. It concludes that the short-time induction heating process works well for reducing surface hardness of the crankshaft. In addition, the 60-seconds induction heating process could

be the intercritical heat treatment from the actual microstructures. However, it still needs to be further proved when it is compared to the microscope microstructures after exact temperature 704 °C and 732 °C induction heating process which are shown in Figure 5-12 and Figure 5-13.

Figure 5-11 Microstructure for 60-seconds Induction Heating Process by SEM (x1500)

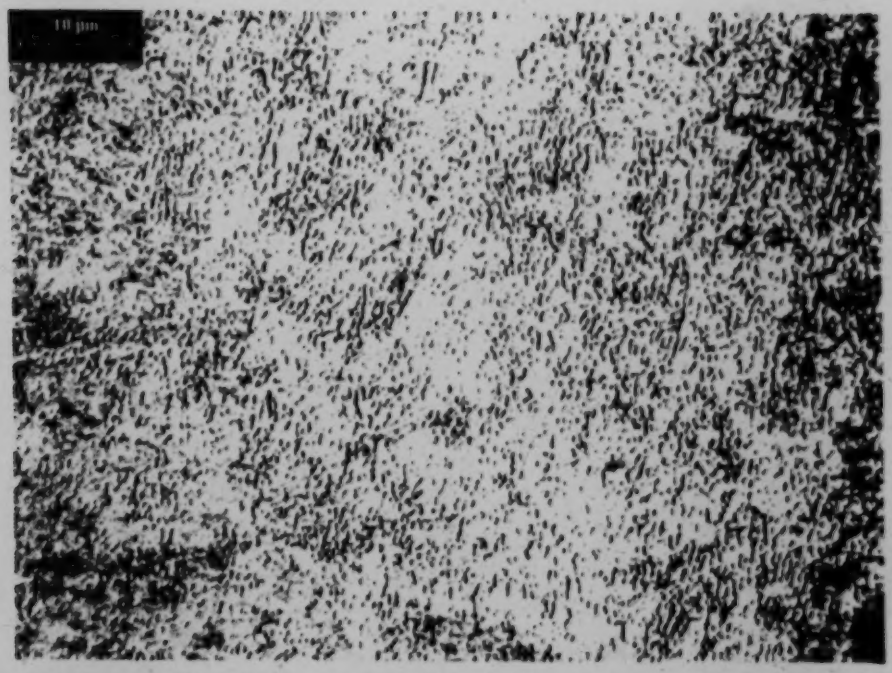

Figure 5-12 Microstructure for Induction Tempering Heat Treatment (704 °C)

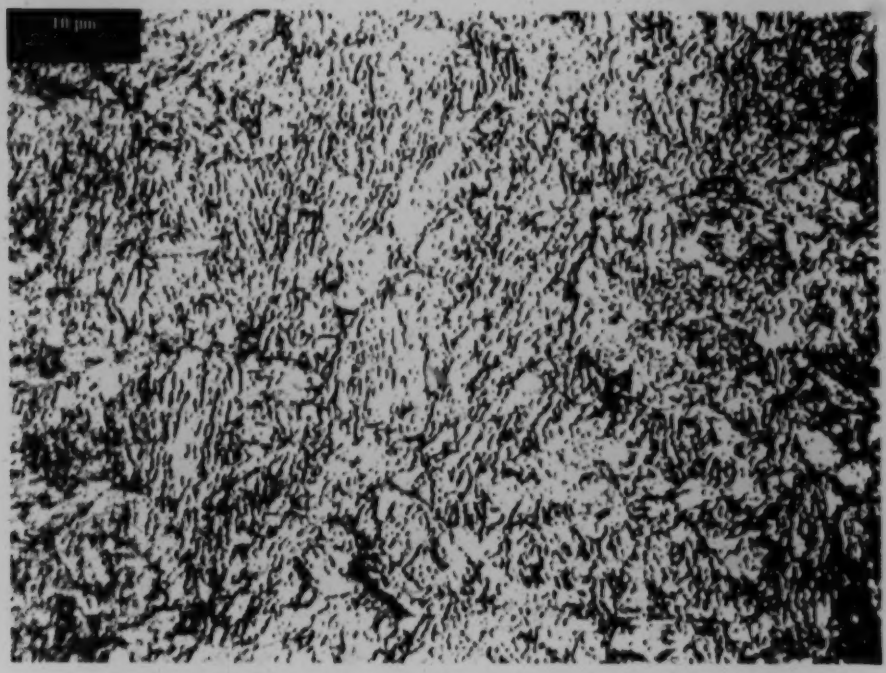

Figure 5-13 Microstructure for Induction Intercritical Heat Treatment (732 °C)

The induction heating process at 704 °C and 732°C are used to investigate difference results from induction tempering and intercritical heat treatment. The crankshaft samples after 704 °C and 732°C induction heating treatment were polished to a 0.05 μm finish and etched in 2% Nital. As the microstructures shown above, the microstructure in Figure 5-12 is typical tempered martensite which is composed of ferrite matrix (bright area) and coarse cementite (dark area). The microstructure in Figure 5-13, ferrite matrix (bright area) with cementite (dark phase) shows in the picture. In addition, there is a little sharp lath-martensite formed in ferrite matrix, and also some retained austenite. The microstructure is very similar to the SEM microstructure for 60-second induction heating process. It proves further that the 60-second induction heat treatment is intercritical heat treatment.

Therefore, from the microstructure and surface hardness analysis, the induction tempering and intercritical heat treatments are both effective to reduce the surface hardness for induction hardened SAE 1040 crankshaft, but the intercritical treatment is the more economic process for industry.

5.5 HVOF

After the induction heating process, the crankshafts journals were grit blasted and coated as required by Headhunters Co for evaluating properties of HVOF coatings. The samples details are as follows:

- Crankshaft journal with induction hardened surface is grit blasted to assess the surface roughness before the induction heat treatment.

- Crankshaft journal with induction hardened surface is grit blasted and then coated by HVOF to assess the properties of the coating before the induction heat treatment.
- Crankshaft journal is induction heated for 60-seconds heating time, then grit blasted to assess the surface roughness after induction heat treatment.
- Crankshaft journal is induction heated for 60-seconds heating time, then grit blasted and coated by HVOF to assess the properties of the coating after the induction heat treatment.

In the following section, experimental investigation on HVOF sprayed coatings was conducted. The mechanical property of the composite coating was evaluated by the tensile test. The coating' microstructures were also studied and evaluated by SEM.

5.5.1 Tensile Test Results and Discussion

The adhesion of the HVOF sprayed coatings to the underlying materials is one of the most important properties of the coatings besides the porosity, hardness and phase distribution. The adhesion of HVOF coatings is determined by standard tensile test followed ASTM C 633-01 standard. The images could determine percentage of the fracture surface still covered by the coating. At the same time, it could be observed the distribution of adhesive and cohesive fracture regions.

The tensile test was run according to the C 633-01 standard test method, but some changes were made for this project to assess the adhesion strength of the HVOF coating. Since the induction intercritical heat treatment is the most effective and economic process

to lower the surface hardness of the crankshaft journal, the crankshaft after 60-seconds induction heating with HVOF coatings was subjected to tensile testing.

For this tensile test, the maximum load applied before rupture occurred was 21 KN (4721 lbF) The drawing of the plug from the coated crankshaft journal caused breaking of the coated layer. In order to reveal the possible reasons for the adhesive strength exhibited, tensile failure morphology of the coatings was analyzed. The fracture surfaces obtained in the tensile test were analyzed by SEM. Figure 5-14 shows the actual image of the fracture surface of this tensile test. The tensile failure in Figure 5-14 is located at the coating / substrate interface rather than within the coatings. And Figure 5-15 and Figure 5-16 show the SEM for fracture surface after tensile test. From these images it can be seen the fracture of the surface is not covered by any of the HVOF coating in this case. It is concluded that the adhesion of the HVOF coating is lower than the tensile strength of the bonding agent – 55 MPa (8000 Psi). The following section calculates the actual adhesive strength for this tensile test.

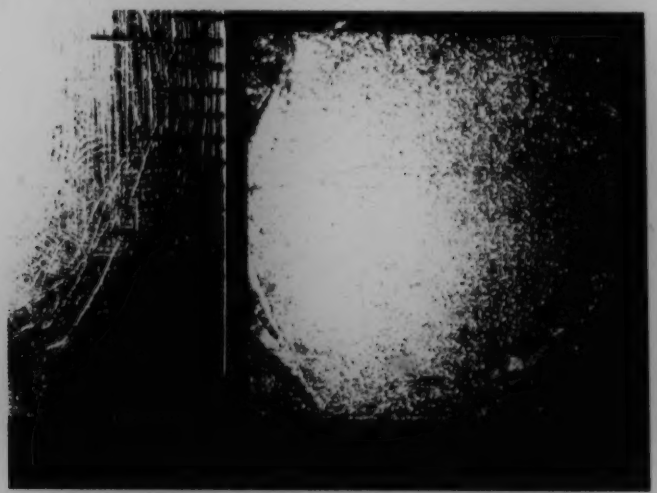

Figure 5-14 Image of Fracture Surface for HVOF Sample after Tensile Test

Figure 5-15 SEM for Fracture Surface after Tensile Test (x400)

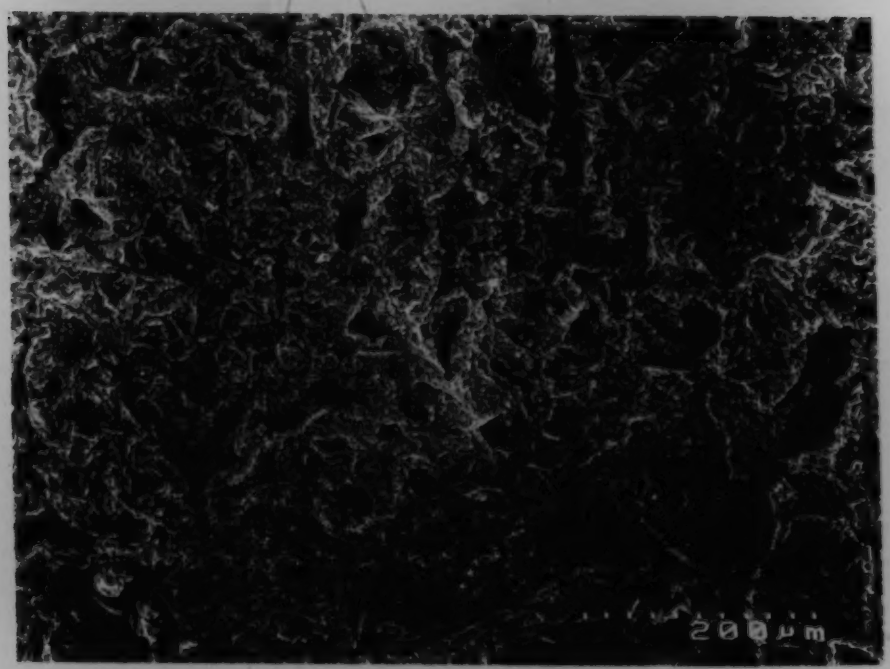

Figure 5-16 SEM for Fracture Surface after Tensile Test (x150)

For calculating the adhesion strength of the HVOF coating, it follows Equation 5-1:

Equation 5-1

Adhesion or Cohesion Strength = maximum load / cross-sectional area

The calculation procedures show below:

- Maximum load applied before the rupture occurred is 21 KN = 4721 lbF
- Cross-sectional area calculation:

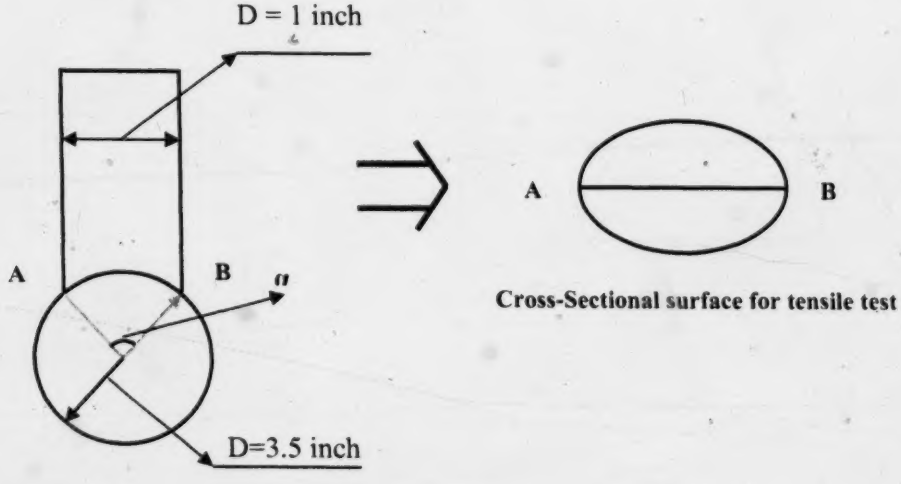

Cross-Sectional surface for tensile test

Actual view for connection between the Crankshaft Journal and loading cylinder

As shown figures above:

$$\text{Sin } \alpha = (0.5) / (3.5/2) = 0.268$$

$$\text{Arc AB} = [(2 \times 16.6°) / 360°] \times \pi \times 3.5 = 1.014 \text{ inch}$$

$$\text{Area of Cross-section} = \pi \times 0.5 \times (1.014 / 2) = 0.7964 \text{ inch}^2$$

Adhesion Strength of HVOF coating = 4721 / 0.7964 = 5928 Psi =41 MPa

The adhesion strength of coating of the crankshaft inducted heated after 60 seconds is about 41 MPa (6000 Psi), which is satisfactory for Headhunters Co.

5.5.2 Crankshaft Journal by Grit Blasting before HVOF Coating

Metal powder coating by HVOF spraying methods are bonded to the substrates by the mechanical interlocking force. To improve the adhesive strength of the coating, the control of the surface geometry of the substrates is one of the important approaches. Grit blasting with alumina is used to roughen the surface in this project. After grit blasting, the substrate surface is modeled by the series of the circular arcs which could supply more attached surface. (Ref. 37)

It is known that the adhesive strength depends on the morphology of the interface between coatings and metal substrates. (Ref. 37, 38, 39) The roughened surface is formed by the plastic deformation which is indented by the impact of hard grit against the substrate surface. Since the SAE 1040 crankshaft journal with induction-hardened surface has very high hardness, the surface could not be roughened properly by the grit blasting. The SEM pictures in Figure 5-17 and Figure 5-18 show the cross-sectional view of the surfaces for the initial surface hardened crankshaft and also the crankshaft surface after induction heat treatment after grit blasting. It is obvious that the surface of initial hardened crankshaft is more flat than the induction heated crankshaft, that is because the surface hardness is lowered greatly after induction heat treatment process, thus becoming much softer. Thus the alumina could blast the surface more effectively and produce more circular arcs on the surface of crankshaft after the surface hardness was reduced. These circular arcs provide more "tooth" for the cladding powder to bond to the surface. Therefore, the induction heat treatment work well for reducing surface hardness to meet the coating surface preparation-grit blasting. (Ref. 40, 41, 42 & 43)

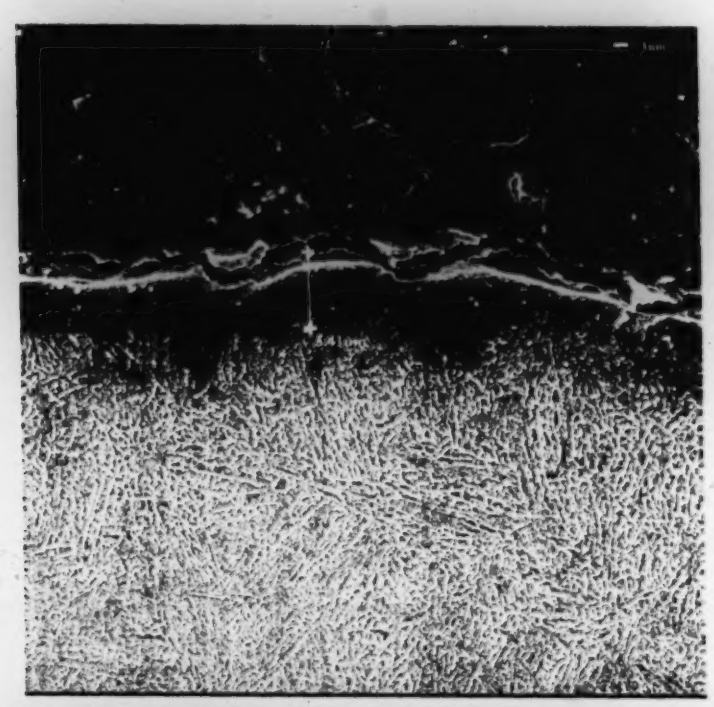

Figure 5-17 Initial Crankshaft after grit blasting

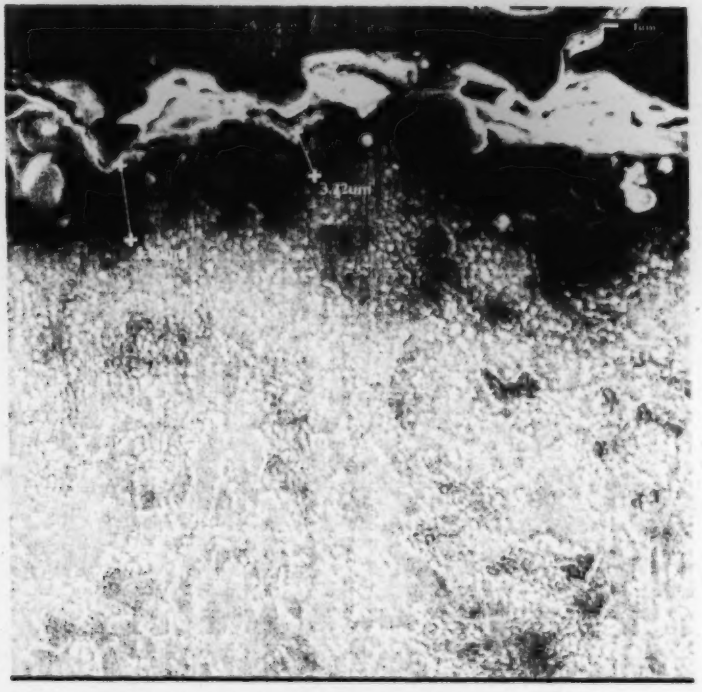

Figure 5-18 Induction-heated Crankshaft after grit blasting

In addition, the SEM image for the morphology of crankshaft surface also verified that the surface roughness of the induction-heated crankshaft is much rougher than the initial surface hardened crankshaft, which is shown in Figure 5-19 and Figure 5-20. From the morphology of both surfaces, the surface of the initial crankshaft give more flat planes, in other words, its surface is smoother. In Figure 5-20, the roughened surface by grit blasting display more circular arcs, which supply more bonding surface area to the coating powder. Thus the surface of induction-heated crankshaft supplies a better roughness for HVOF coating. Since the adhesive strength of HVOF coating is related to the contact area between coatings and substrates, the adhesive strength of the coating is obviously improved after induction heat treatment.

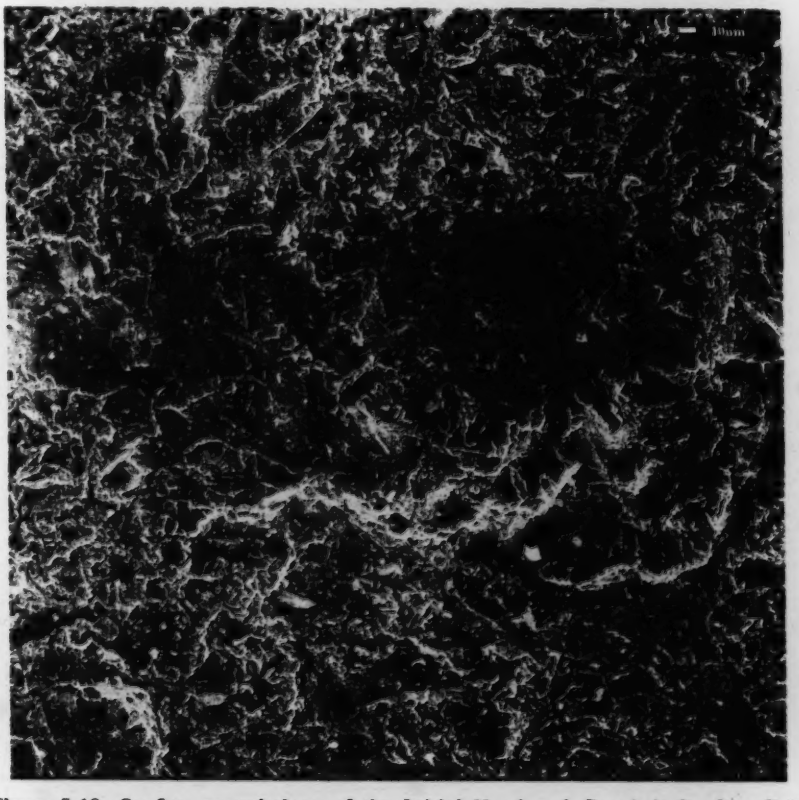

Figure 5-19 Surface morphology of the Initial Hardened Crankshaft after Grit Blasting (x200)

Figure 5-20 Surface morphology of the Induction Heated Crankshaft after Grit Blasting (x200)

5.5.3 HVOF Coatings Properties

High Velocity Oxy-Fuel (HVOF) spray deposition processes are one of today's most active and growing areas in thermal spray coating technology. The primary characteristic of HVOF processes is dense, high quality metal, coatings using combustion as the heat source. The microstructure of HVOF coating consists of oriented lamellae in the plane of the substrate. Typical commercially HOVF spray coatings may contain varying degrees of porosity and oxide scales, and unmelted and partially melted particles are also common. (Ref. 44, 45 & 46)

The properties of the coating were studied by evaluating hardness, structure of cross section, and limitation of coating thickness. (Ref. 47 & 48) The crankshaft sample coated after 60-seconds induction heating with coating was analyzed. Distribution of composition and porosity across the cross section were observed on a polished coating cross-section by using scanning electron microscopy (SEM). Cross sectional SEM photomicrographs of HVOF coating are shown in Figure 5-21, Figure 5-22 and Figure 5-23 with different magnifications, and oriented with the substrate at the bottom. Hardness of the coating surface and cross section were measured by Microhardness tester DATA LETTY 150.

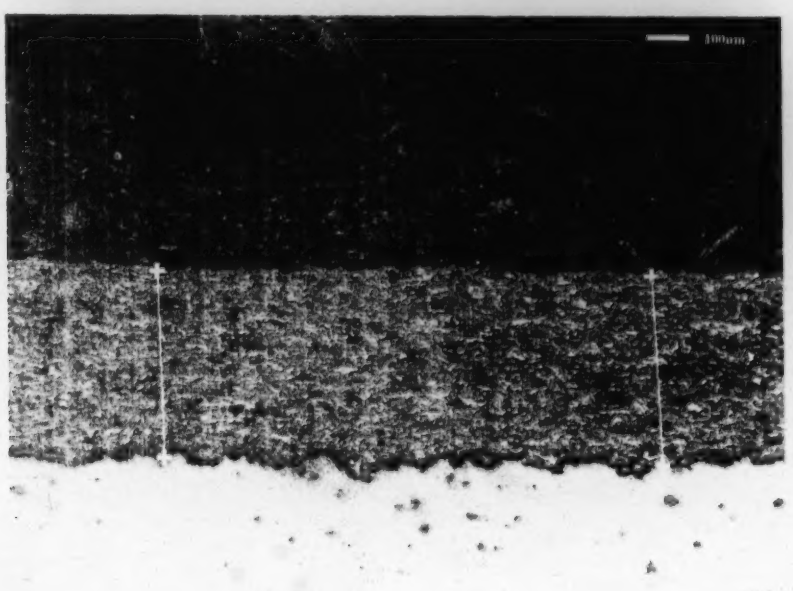

Figure 5-21 Cross Sectional Scanning Electron Micrograph of the as-sprayed coatings (x 50)

The SEM image of Figure 5-21 shows the HVOF coating in transverse sections. The coating thickness is about 440 μm. The coating images of Figure 5-22 and Figure 5-23 (same coating but different magnifications) show that, the HVOF coating layer contains oxide (gray) and metal (white) phase, porosity (black) and some partially melted particles visibly deformed on impact. The matrix alloy and coating powder are bonded well, the metal coating powder is dispersed uniformly, and all the particles form good lamellae. There are no cracks. Figure 5-23 also displays more clearly that good packing density with very little unmelted or resolidified particles in the coating. This is a typical layered structure presented as gray oxide stringers between the lamellae. This indicates oxidation of the molten particles in transit to the substrate. The microstructure result shows that the HVOF coating of the induction-heated crankshaft is stable.

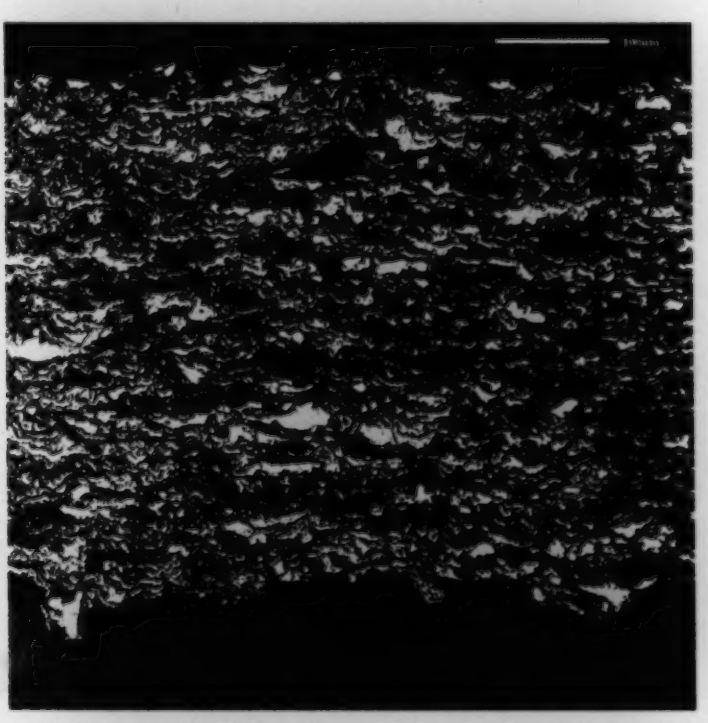

Figure 5-22 Cross Sectional Microstructure of Interface layer between HVOF coating and Crankshaft Surface (x 150)

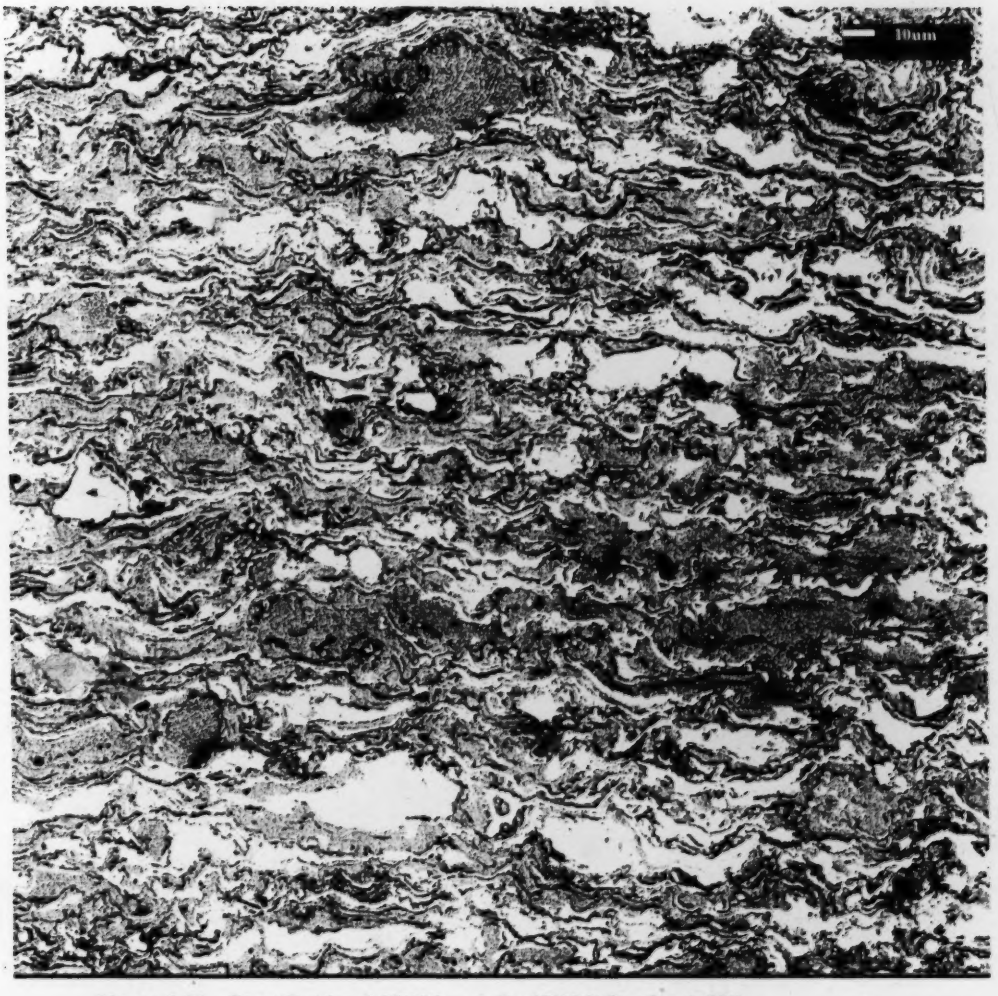

Figure 5-23 Cross Sectional SEM image for HVOF Coating (x300)

The surface hardness of the HVOF coating is 900 Hv and the hardness of the cross section is 946 Hv, which were measured by microhardness tester, the load for testing is 500 g. Therefore, there is not much decrease in hardness from the bottom coating layer to the top coating layer and the variation is low. The surface morphology by SEM of the same sample with coating is shown in Figure 5-24. A top view of the as-sprayed deposit reveals platelet-shaped particle incorporating a large amount of surface debris. It shows

no porosity. It reveals that clean powder interfaces, and homogeneous, uniform structures are obtained throughout the coatings.

The analysis of the properties of the HVOF coating for the coated surface of the induction heated crankshaft shows the surface coating is stable with high adhesion strength, and good wear resistance due to the high surface hardness, in addition a good bonding coating.

For this particular project, the worn crankshaft journal with induction hardened surface could be remanufactured by HVOF process after it is induction heat-treated. And the coating properties is qualified.

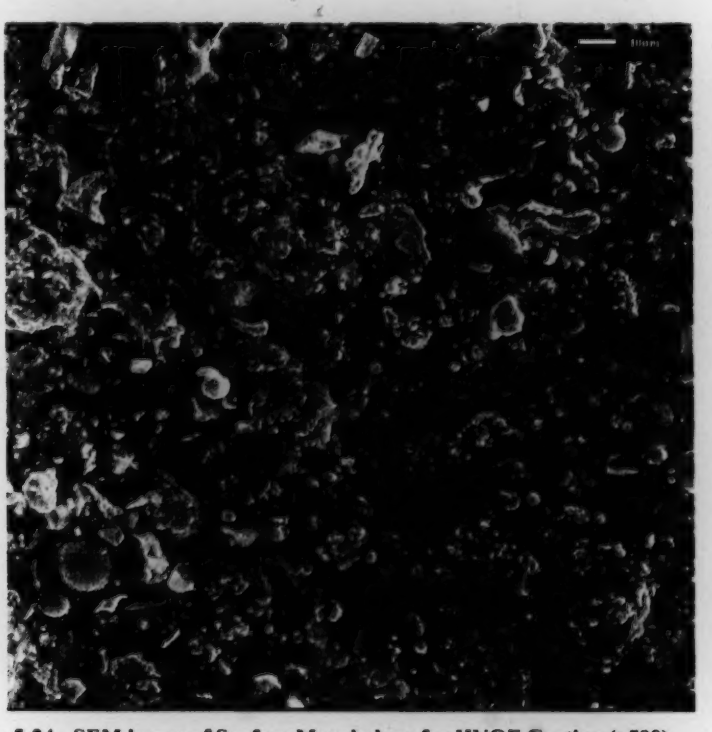

Figure 5-24 SEM image of Surface Morphology for HVOF Coating (x500)

6 Conclusions

Based on the work carried out in this project, the following conclusions about the SAE 1040 induction hardened crankshaft journal can be made:

1. Worn SAE 1040 crankshaft journals with induction hardened surface can be remanufactured by HVOF coating after 60 seconds induction intercritical heat treatment. The adhesive strength of coating and coating properties are satisfactory for the industry.

2. Both induction tempering and induction intercritical heat treatment can reduce surface hardness of crankshaft journal appropriately, using a radio frequency induction furnace. The induction heating time is quite short (for tens seconds), which is very economic and practical for the industry.

3. The conventional short-time furnace treatment could lower the surface hardness to an acceptable value. The martensite zone is tempered and transformed to ferrite with coarse cementite.

4. Less conventional short-time intercritical furnace heat treatment is also effective to reduce the surface hardness significantly. In the intercritical annealing, some austenite will be formed in the structure. The brittle and hard martensite phase in the surface is softened by transforming to ferrite, cementite and retained austenite after intercritical heat treatment.

5. For induction tempering heat treatment, the products are ferrite and coarse cementite which are same as the furnace tempering treatment. However, for intercritical induction heat treatment, the products are ferrite, cementite, retained austenite, and very little martensite formed due to the rapid cooling rate in induction heating treatment.

6. Intercritical induction heat treatment is proved to be more effective for lowering surface hardness to produce a surface which may be roughened by grit blasting. The required sixty seconds of induction heating time is very economical and practical for the industry.

7. The properties of HVOF coating were evaluated for the crankshaft after induction intercritical heat treatment. The adhesion strength of the coating is about 41 MPa which satisfied the Headhunter Co. The SEM images for surface morphology and cross section of the coating show that the HVOF coating is very stable and homogeneous, with low porosity.

8. The initial hardness of SAE 1040 induction hardened crankshaft is about 530 Hv. The crankshaft samples by different induction heating process were hardness tested, and the samples show hardness reductions of more than 230 Hv. Then the samples were grit blasted and the surface was inspected in the scanning electron microscope (SEM). Grit blasting provides good surface and produces sufficient

"tooth" for HVOF coating integrity. Therefore, the tolerable surface hardness for the required HVOF thermal treatment is about 300 Hv.

9. In order to determine the adhesion strength of HVOF coating, tensile tests were different from the ASTM C633-01 standard method which was conducted on the round surface of the crankshaft journals. With the special self-aligning device and the cylindrical loading fixture with the curved end, a good assessment of the adhesion strength for spherical surface with coating was achieved.

10. In the heating temperature measurement for the induction heat-treating process, the thermocouple is not a good choice since the metallic thermocouple junction is experiences eddy currents from the radio frequency induction furnace, thus causing inaccurate temperature records. The infrared pyrometer is a optional device for temperature measurement since the spot diameter must be smaller than the gap length between the induction coils. Tempil sticks provide a practical device for temperature measurement in this project, but cannot give the precise temperature value.

7 Recommendations for Future Research

The following are recommendations for further study:

- For the temperature measurement of induction heat-treating process, the exact temperature was not achieved for each induction heating in this project. Future research should find a good temperature measurement device which could get the precise value.

- In addition, in the project the worn crankshafts often are cracked and must be repaired before HVOF coating is sprayed on. Therefore, repair welding needs to be investigated for its effect in the future, not only on the repair itself, but also on the hardness profile of the induction hardening, since "tooth" produced by grit blasting may be different in areas thermally cycled in the welding procedure.

8 Reference

1 http://www.airliquide.com/en/business/industry/welding/application/coating_oxyfuel.asp, August 2003

2 Brian Guske, "High Velocity Oxy-Fuel Spray Technology", http://www.dresser-rand.com/e-tech/PDF%20Files/tp106.pdf, 2003

3 R.W. Smith, "Equipment and theory, Lesson from Thermal Spray Technology", Course 51, Materials Engineering Institute, ASM International, Materials Park, Ohio, USA, 1992

4 Fushui Wei, Boping Jiang, Xingkai Wang and Junyue Li, "Thermal Spray Technology", Mechanical Industry Publishing House, P.R.China, June 1985, P 56-61

5 M. Jackson, J. Rairden, J. Smith, and R.W. Smith, *J. Metals*, Vol. 1, 1981, P 146

6 http://www.hvof.com/index.html, August 2003

7 B.M. Patchett, The Metals Blue Book, *Welding Filler Metals*, Second Version, CASTI Publishing Inc., Edmonton, Canada, P 51

8 Robert E. Reed-Hill and Reza Abbaschian, *Physical Metallurgy Principles*, Third Edition, P 588

9 http://www.geocities.com/SiliconValley/Campus/8262/htdocs/steels/indx.html, August 2003

10 T. Tanaka, *High Strength Low Alloy Steels*, D.P. Dunne and T. Chandra, Ed., South Coast Printers, Port Kembla, Australia, 1985, P 7

11 Robert E. Reed-Hill, *Physical Metallurgy Principles*, second version, D. VAN NOSTRAND Company, INC., Princeton, New Jersey, USA, 1992, P 439-476

12 W. Smith, 1993, *Structure and Properties of Engineering Alloys*, Second Edition, Mcgraw Hill P129-132, 1993

13 Adapted from H. Boyer, Editor, *Atlas of Isothermal Transformation Diagrams*, American Society for Metals, Materials Park, Ohio, USA, 1977, P 369

14 D. Williams JR. Callister, *Materials Science and Engineering-An Introduction* Fifth version, P 281-357, 2000

15 *After Metals Handbooks*, 9th ed., vol. 8, American Society of Metals, Materials Park, Ohio, USA, 1973, P 191

16 P.R. Mould, in *Metallurgy of Continuous-Annealed Sheet Steel*, B.L. Bramfitt and P.L. Mangonon, Ed., TMSAIME, 1982, P 3-33

17 Metals Handbook, Vol. 8, 8th edition, *Metallography Structures and Phase Diagrams*, American Society for Metals, Materials Park, OH, 1973

18 A.R. Marder and G. Krauss, *Trans.* ASM 60: 651, Materials Park, Ohio, USA, 1967

19 William F. Smith, *Structure and Properties of Engineering Alloys*, Second Edition, P 26-39, 1993

20 Metals Handbook, Vol. 9, 9th edition, *Metallography and Microstructures*, American Society for Metals, Materials Park, OH, 1985

21 P.A. Hassell and N.V. Ross, "Induction Heat treating of Steel", *Heat Treating*, Vol.4, *ASM Handbook*, 1991, P 164-202

22 S. Lampman, "Introduction to Surface Hardening of Steels", *Heat Treating*, Vol. 4, *ASM Handbook*, 1991, P 259-267

23 S.L. Semiatin and D.E. Stutz, "Induction Heat Treatment of Steel", *ASM Handbook*, 1986, P 51-60

24 A.D. Demichev, *Surface Induction Hardening*, St. Petersburg, Russia, 1990 (in Russian")

25 G.F Golovin and M.M. Zamjatin, "High-Frequency Induction Heat Treating", Mashinostroenie, St. Petersburg, Russia, 1990 (in Russian)

26 "ASTM Standard C 633-01", *Annual book of ASTM Standard*, Vol. 03.01, ASTM International, P 771-777, 2001

27 INDUCTOHEAT Bulletin, "Hardening and Tempering of Automotive Spindles", 1991

28 ASM, Metals Handbook, 9th ed., Vol. 4, *Heat Treating*, ASM, Cleveland, OH, P 164-202, 1991

29 INDUCTOHEAT Bulletin, "A New Wave of Induction Hardening Automation", 1992

30 OMEGA Infrared Pyrometer Manual, OMEGA Inc., 2003

31 P.D. Bilmes, M. Solari and C.L Llorente, "Characteristics and effects of austenite resulting from tempering of 13Cr-NiMo martensite steel weld metals", *Materials Characterization* 46 (2001) P 285-296

32 K. Forch, W. Witte, Hattingen, S.B., "Application of three-stage heat treatment to thick-walled workpieces from weldable, high-strength fine-grained structural steels and reactor steels", Stahl u. Eisen, P 100, 1329-1338, 1980

33 K.D. Haverkamp, K. Forch, K. -H. Piehl, W. Witte, "Effect of heat treatment and precipitation state on toughness of heavy section Mn-Mo-Ni-steel for nuclear power plants components", *Nuclear Engineering and Design*, P 81, 207-217, 1984

34 H. Huang, O. Matsumura and T. Furukawa, "Retained austenite in low carbon, manganese steel after intercritical heat treatment", *Materials Science and Technology (UK)*, vol. 10, no. 7, pp. 621-626, July 1994

35 Byeong-Joo Lee, Hong-Deok Kim and Jun-Hwa Hong, "Calculation of α/γ Equilibria in SA508 Grade 3 Steels for intercritical Heat Treatment", *Metallurgical and Materials Transactions A*, Volume 29A, May 1998, P 1441-1447

36 Valery I. Rudnev, Raymond L. Cook, Don L. Loveless and Micah R. Black, "Induction Heat Treatment, Basic Principles, Computation, Coil Construction, and Design Considerations", *Steel Heat Treatment Handbook*, Edited by George E. Totten, Union Carbide Corporation, Tarrytown, New York, 1997, P 785

37 E. Nozi, et al., 45th Conference of Jap. Thermal Spraying Soc., P 70-76, 1986 (in Japanese)

38 K. Tani, et al., Memoirs of Niihama National College of Tech. (Sci. and Eng.), P 23, 127-134, 1987 (in Japanese)

39 K. Hiraki, Kyushuu Sangyou Gijutsu, P 9, 67-74, 1988, (in Japanese)

40 S. Amada, H. Yamada, S. Yematsu and Y. Saotome, "Modelling and Measurements of Adhesive Strength of Thermal Sprayed Coatings", *Proceedings of the International Thermal Spray Conference & Exposition*, Orlando, Florida, USA, 28 May – 5 June, 1992 P 915-920

41 W. Han, E.F. Rybicki and J.R. Shadley, "Bond Strength Testing of Thermal Spray Coatings Using ASTM C633-79: Effect of Specimen Size on Test Results", *Proceedings of the International Thermal Spray Conference & Exposition*, Orlando, Florida, USA, 28 May – 5 June, 1992 P 911-914

42 J.C. Vazquez and A. Scagni, "Heavy Duty Crankshaft Reclamation, A thermal Spray Coating Evaluation", *Proceedings of the Fourth National Thermal Spray Conference*, Pittsburgh, PA, USA, 4-10 May 1991, P 153-158

43 Jeannie D. Haman, Krishnan K. Chittur, Daryl E. Crawmer and Linda C. Lucas, "Analytical and Mechanical Testing of High Velocity Oxy-Fuel Thermal Sprayed and Plasma Sprayed Calcium Phosphate Coatings", *Journal of biomedical materials research*, 48(6):P 856-860, 1999

44 R. Knight and R.W. Smith, "HVOF Spray 80/20 NiCr Coatings-Process Influence Trends", *Proceedings of the International Thermal Spray Conference & Exposition*, Orlando, Florida, USA, 28 May – 5 June, 1992 P 159-164

45 L.N. Moskowitz, "Application of HVOF Thermal Spraying to Solve Corrosion Problems in the Petroleum Industry", *Proceedings of the International Thermal Spray Conference & Exposition*, Orlando, Florida, USA, 28 May – 5 June, 1992 P 611-318

46 C.C. Berndt, J. Karthikeyan, R. Ratnaraj and Y.D. Jun, "Material Property Variations in Thermally Sprayed Coatings", *Proceedings of the Fourth National Thermal Spray Conference*, Pittsburgh, PA, USA, 4-10 May 1991, P 199-203

47 M. Sasaki, F. Kawakami, C. Komaki and M. Ishida, "Characterization of HVOF Sprayed Cr_3C_2 Coating", *Proceedings of the International Thermal Spray Conference & Exposition*, Orlando, Florida, USA, 28 May – 5 June, 1992 P 165-170

48 Xiao-xi Guo and Hong Zhang, "HVOF-Sprayed Tribaloy (T-800): Microstructure and Particle-Erosion Behaviour", *Proceedings of the International Thermal Spray Conference & Exposition*, Orlando, Florida, USA, 28 May – 5 June, 1992 P 729-734